https://doi.org/10.5194/cp-2024-10
Preprint. Discussion started: 12 February 2024

Climate of the Past Discussions

Contrasting the Penultimate and Last Glacial Maxima (140 and 21 ka BP) using coupled climate-ice sheet modelling

Violet L. Patterson[1], Lauren J. Gregoire[1], Ruza F. Ivanovic[1], Niall Gandy[2], Jonathan Owen[1], Robin S. Smith[3], Oliver G. Pollard[1], Lachlan C. Astfalck[4]

[1]School of Earth and Environment, University of Leeds, Leeds, UK
[2]Department of the Natural and Built Environment, Sheffield Hallam University, Sheffield, UK
[3]NCAS, Department of Meteorology, University of Reading, Reading, UK
[4]School of Physics, Mathematics and Computing, University of Western Australia, Perth, Australia

Correspondence to: Violet L. Patterson (ee17vp@leeds.ac.uk)

Abstract. The configuration of the Northern Hemisphere ice sheets during the Penultimate Glacial Maximum differed to the Last Glacial Maximum. However, the reasons for this are not yet fully understood. These differences likely contributed to the varied deglaciation pathways experienced following the glacial maxima and may have had consequences for the interglacial sea level rise. Therefore, a better understanding of how and why these two glacial maxima differed is crucial for developing the full picture on why the Last Interglacial sea level was up to 9 meters higher than today, and thus may help constrain future sea level rise. To understand the differences between the North American Ice Sheet at the Last and Penultimate Glacial Maxima (21 and 140 ka BP), we perform two perturbed-physics ensembles of 62 simulations using a coupled climate-ice sheet model FAMOUS-ice, in which the North American and Greenland ice sheets are dynamically simulated with the Glimmer ice sheet model. We select six ensemble members that match reconstructed ice extent and volumes at the Last and Penultimate Glacial Maxima. To understand the role of orbit, greenhouse gases and initial conditions on the final ice sheet configurations, we use a factor decomposition technique. This reveals that the initial ice sheet conditions used in the model are extremely important in determining the difference in final ice volumes between both periods due to the large effect of the ice-albedo feedback. In contrast to evidence of a smaller Penultimate North American Ice Sheet, our model shows that the climate boundary conditions at these glacial maxima, if considered in isolation, imply a larger Penultimate Glacial Maximum North American Ice Sheet than at the Last Glacial Maximum, of around 6 meters sea level equivalent. This suggests the growth of the ice sheet prior to the glacial maxima is key in explaining the differences in North American ice volume.

1 Introduction

The Penultimate Glacial Maximum (PGM) occurred around 140,000 years ago, within Marine Isotope Stage 6 (MIS 6). Greenhouse gas (GHG) concentrations and global average insolation were similar to the Last Glacial Maximum (LGM; ~21 ka BP) (Berger and Loutre, 1991; Loulergue et al., 2008; Bereiter et al., 2015) but the orbital configuration differed, affecting the seasonal and latitudinal distribution of incoming shortwave radiation (Berger, 1978; Colleoni et al., 2011). The global total

https://doi.org/10.5194/cp-2024-10
Preprint. Discussion started: 12 February 2024

ice sheet volume, and thus the global mean sea level, was likely similar between the two glacial maxima (~120-130 m below present), with larger uncertainty at the PGM (Rabineau et al., 2006; Masson-Delmotte et al., 2010; Rohling et al., 2017). Both geological evidence and numerical modelling suggest that despite the similarities in total ice volume between the PGM and the LGM, the configurations of the Northern Hemisphere ice sheets differed significantly (e.g. Svendsen et al., 2004; Colleoni et al., 2016; Batchelor et al., 2019).

Some reconstructions suggest the Eurasian Ice Sheet (EIS) may have been up to ~50 % larger during the Penultimate Glacial Cycle (MIS 6: ~190-130 ka BP) than during the Last Glacial Cycle (~115-12 ka BP) (Svendsen et al., 2004), however evidence of multiple advances and uncertainties in dating proxy records means that the maximum extent mapped at 140 ka BP could correspond to previous advances during MIS 6 (Svendsen et al., 2004; Margari et al., 2014; Colleoni et al., 2016; Ehlers et al., 2018). The extent of the North American Ice Sheet (NAIS) during the PGM is even less well constrained due to a lack of glaciological evidence (e.g. moraines and till). The scarcity of empirical data in itself suggests that it was smaller in most areas than at the LGM because the subsequent larger ice sheet could have largely erased the evidence of prior glaciations (Dyke et al., 2002; Rohling et al., 2017). Additionally, evidence of reduced ice rafted debris (IRD) discharge from the Hudson Strait in the North Atlantic IRD belt (e.g. Hemming, 2004; Naafs et al., 2013; Obrochta et al., 2014), relative sea level assessment studies (e.g. Rohling et al., 2017) and climate, ice sheet and glacial isostatic adjustment modelling (e.g. Colleoni et al., 2016; Dyer et al., 2021) all point to a smaller volume PGM NAIS. For example, assuming a similar global mean sea level fall (and Antarctic ice sheet volume) at the PGM as at the LGM but with a larger volume EIS at the PGM (estimated at 33-53 m sea level equivalent (SLE) versus 14-29 m SLE at the LGM), this follows that the NAIS must have been smaller than at the LGM to compensate (39-59 m SLE versus 51-88 m SLE) (Rohling et al., 2017).

The reason for these differences is likely complex and is not yet fully understood. The evolution and surface mass balance (SMB) of ice sheets depends on many factors such as; background climate, climate and ice sheet histories, dust deposition, vegetation, ice albedo and sea surface temperatures, as well as the interactions and feedbacks between them all (Kageyama et al., 2004; Krinner et al., 2006; 2011; Colleoni et al., 2009a; 2011; Liakka et al., 2012; Stone and Lunt, 2013). The ice sheets themselves also strongly influence the climate through their interactions with atmospheric and oceanic circulation and the energy balance. This alters global and local temperature and precipitation patterns which in turn affects ice sheet ablation and accumulation (i.e. SMB) (e.g. Kageyama and Valdes, 2000; Abe-Ouchi et al., 2007; Beghin et al., 2014; 2015; Ullman et al., 2014; Liakka et al., 2016; Gregoire et al., 2015; 2018; Snoll et al., 2022; Izumi et al., 2023). These interactions between the vast ice sheets and other components of the climate system exerted an important control on the initial climate state for the deglaciations, and hence on the subsequent chain of events, thus impacting the climate, ocean and sea level evolution during deglaciation. Thus, the contrasting configurations of the Northern Hemisphere ice sheets at the glacial maxima may have contributed to the different deglaciation pathways that followed. The timings and magnitudes of the climate and ocean circulation changes that occurred during the Penultimate Deglaciation (~138-128 ka BP) differed to the Last Deglaciation (~19-11 ka BP) (Landais et al., 2013; Menviel et al., 2019). For example the Last Deglaciation experienced two abrupt climate

https://doi.org/10.5194/cp-2024-10
Preprint. Discussion started: 12 February 2024

changes associated with a weakened Atlantic Meridional Overturning Circulation, Heinrich Stadial 1 and the Younger Dryas (Denton et al., 2010; Ivanovic et al., 2016; 2018), compared to evidence of only one, much longer abrupt change towards the end of the Penultimate Deglaciation, Heinrich Stadial 11 (Cheng et al., 2009; Govin et al., 2015; Marino et al., 2015; Jimenez-Amat and Zahn, 2015). The deglaciations also led to interglacials with very different characteristics to one another, including average global surface temperatures 1-2 °C higher and sea level up to 9 m higher than the pre-industrial during the Last Interglacial (~129-116 ka BP) (Kopp et al., 2009; Turney and Jones, 2010; Grant et al., 2012; Dutton and Lambeck, 2012; Otto-Bliesner et al., 2013; Dutton et al., 2015; Dyer et al., 2021).

In this context, it is important to examine the complex physical interactions between the climate and the ice sheets to better understand why the last two glacial maxima had different ice sheet configurations and evaluate the ice sheets' sensitivities to changes in climate in relation to different orbits and greenhouse gas concentrations.

Despite the challenges in coupling Atmosphere Ocean General Circulation Models (AOGCMs) with ice sheet models due to the mismatch between the required spatial and temporal scales, recent technical advances have meant that this is now possible. A combination of increased computer power, the development of more computationally efficient, lower resolution AOGCMs and sub-grid scale schemes translating ice sheet relevant atmospheric processes onto the higher resolution ice sheet grid, has made bi-directional, coupled climate-ice sheet simulations over longer timescales, and in large ensembles, feasible (Fyke et al., 2011; Vizcaino et al., 2013; Ziemen et al., 2014; Sellevold et al., 2019; Smith et al., 2021).

This study uses a coupled climate-ice sheet model, called FAMOUS-ice (Smith et al., 2021), to perform ensemble simulations of the PGM and LGM to explore input climate and ice sheet parameter uncertainties, their effects on the North American ice sheet volume during each period, and find parameter combinations that give a reasonable ice sheet configuration for both glacial maxima. The ensembles are also constrained based on volume and extent metrics and the 'Not Ruled Out Yet' (NROY) simulations are analysed to try and understand the similarities and differences between both periods. We find that the initial conditions used in the LGM and PGM experiments played an important role in some of the differences seen and we quantify this impact through the use of sensitivity tests and factor decomposition analysis.

2 Methods

2.1 Model description

FAMOUS is a fast, low resolution AOGCM that is based on Hadley Centre coupled model HadCM3 and therefore retains all the complex processes represented in an AOGCM but uses only half the spatial resolution and a longer time step. Since it requires only 10 % of the computational costs of HadCM3, it has been successfully used for long transient palaeo simulations (Smith and Gregory, 2012; Gregory et al., 2012; Gregoire et al., 2012; Roberts et al., 2014; Dentith et al., 2019) and large ensembles for uncertainty quantification (Gregoire, 2010; Gandy et al., 2023). This study uses the atmospheric component, which is a quasi-hydrostatic, primitive equation grid point model with a horizontal resolution of 7.5° longitude by 5° latitude

https://doi.org/10.5194/cp-2024-10
Preprint. Discussion started: 12 February 2024

Climate of the Past Discussions

with 11 vertical levels and a 1-hour time step (Williams et al., 2013). Land processes are modelled using the MOSES2.2 land surface scheme (Essery et al., 2003), which uses a set of sub-gridscale tiles in each grid box to represent fractions of nine different surface types, including land ice (Smith et al., 2021). Whilst this study prescribes sea surface temperatures and sea ice concentrations, FAMOUS can also be run fully coupled with a dynamical ocean (e.g. Dentith et al., 2019).

FAMOUS now allows the direct two way coupling to an ice sheet model in the configuration FAMOUS-ice (Smith et al., 2021). Here, we use FAMOUS in combination with Glimmer to interactively simulate the North American and Greenland ice sheets at 40km resolution. Glimmer is a fast running, 3D thermomechanical ice sheet model which uses the shallow ice approximation. This allows it to model ice sheet evolution over long timescales as it is more computationally efficient, and therefore has been used to simulate continental ice sheets over glacial-interglacial cycles (Rutt et al., 2009; Gregoire et al., 2016).

FAMOUS-ice accounts for the mismatch between atmosphere and ice sheet grid sizes by using a multilayer surface snow scheme to calculate SMB on 'tiles' at 10 set elevations within each grid box that contains land ice in FAMOUS. This SMB is then downscaled from the coarse FAMOUS grid to the much finer Glimmer grid at each model year (Smith et al., 2021). Glimmer uses this SMB field to calculate ice flow and surface elevation and passes this back to FAMOUS in which orography and ice cover is updated. In this study, to reduce computational costs further, FAMOUS-ice runs at 10 times ice sheet acceleration: for every year of climate integrated in FAMOUS, the simulated SMB field forces 10 years of ice sheet integration in Glimmer. Figure 1 shows a simplified diagram of this coupling process and full details can be found in Smith et al., (2021). The current computational cost of this set up is around 50 decades (of climate years) per wallclock day using 8 processors.

FAMOUS-ice has been shown to perform well in simulations of past and future ice sheets including Greenland and North America (Gregory et al., 2020; Smith et al., 2021; Gandy et al., 2023). In particular, the LGM North American Ice Sheet study of Gandy et al., (2023) was able to utilise the useful constraints of the LGM to infer the importance of parameters controlling ice sheet albedo on ice sheet configuration in this model.

https://doi.org/10.5194/cp-2024-10
Preprint. Discussion started: 12 February 2024

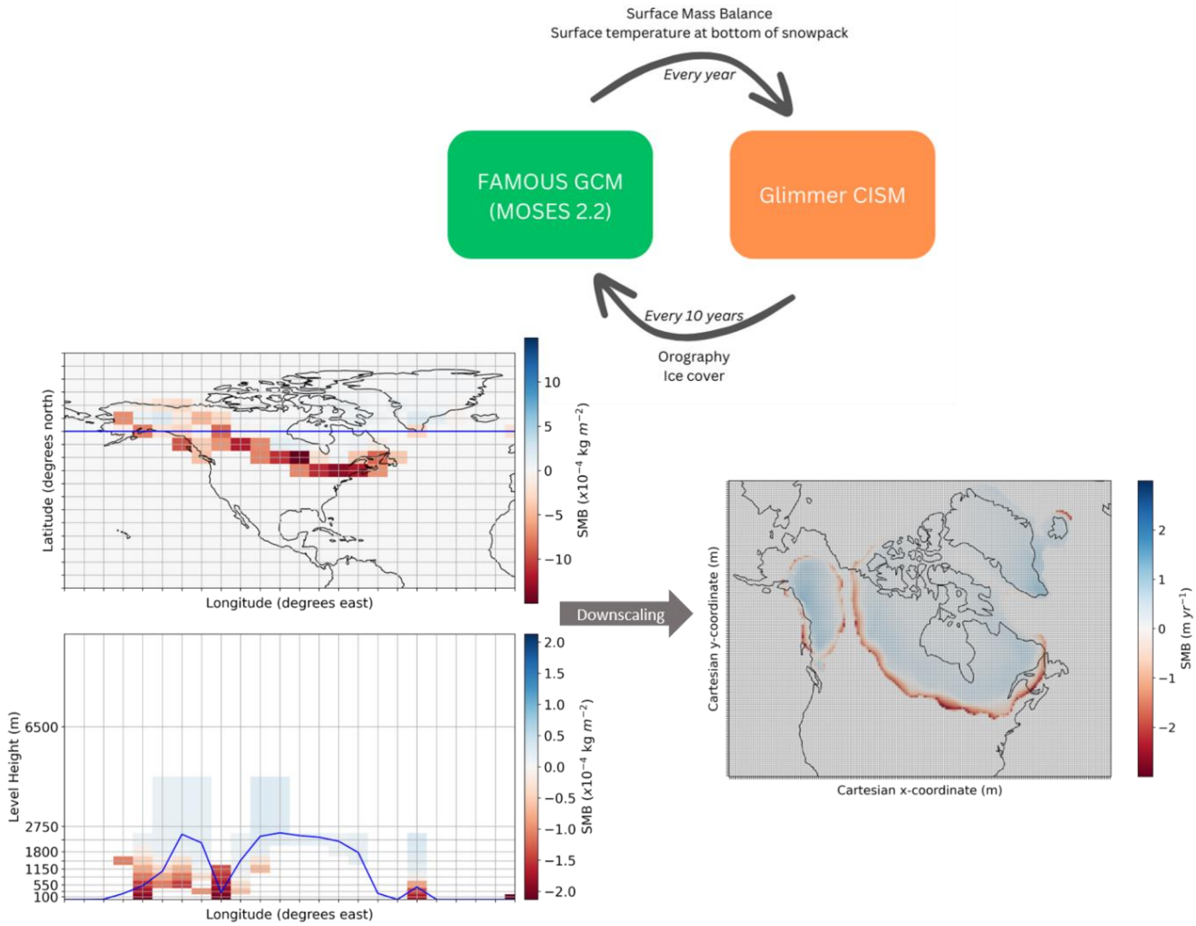

Figure 1. Schematic illustrating the calculation of SMB at different elevations on the FAMOUS grid followed by downscaling onto the Glimmer grid.

2.2 Experiment design

Our FAMOUS-ice simulations are set up following the Paleoclimate Modelling Intercomparison Project Phase 4 (PMIP4) protocols for the LGM (Kageyama et al., 2017) and PGM (Menviel et al., 2019). These protocols prescribe climatic boundary conditions, including orbital parameters and GHG concentrations, the values of which can be found in Table 1. Concentrations of CO_2, CH_4 and N_2O are very similar between the LGM and PGM but orbital parameters are significantly different. The larger eccentricity at the PGM enhances the effect of precession compared to the LGM which affects the seasonal and latitudinal distribution of insolation. These changes are important for ice sheet surface mass balance since melting is particularly sensitive to spring and summer temperatures (Huybers, 2006; Niu et al., 2019). The PGM received lower insolation in the Northern Hemisphere in late winter to early summer but higher levels in late summer to early winter, compared to the LGM (Fig. 2a). Subsequent to the completion of this work, it was discovered that the equation for the role of eccentricity on solar insolation

https://doi.org/10.5194/cp-2024-10
Preprint. Discussion started: 12 February 2024

was incorrect in the model code. The magnitude of the error is larger for periods with higher eccentricity values and so a sensitivity test was run to determine the effect this correction has on SMB and ice volume at the PGM. Details of this error and the results of the sensitivity test can be found in Appendix A, but the impact was shown to be minimal (Fig. A1).

Table 1. Climatic boundary conditions used in the LGM and PGM experiments as prescribed by the PMIP4 protocols for each period (Kageyama et al., 2017; Menviel et al., 2019).

	Eccentricity	*Obliquity (°)*	*Perihelion – 180 (°)*	*Solar Constant (Wm^{-2})*	*CO_2 (ppm)*	*CH_4 (ppb)*	*N_2O (ppb)*
LGM (21 ka)	0.019	22.949	114	1360.7	190	375	200
PGM (140 ka)	0.033	23.414	73	1360.7	191	385	201

In the climate model, the global orography (including ice sheets) and land-sea mask for the LGM are calculated from the GLAC1D 21 ka BP reconstruction (Tarasov et al., 2012) which is one of the two options in the PMIP4 protocol (Kageyama et al., 2017). For the PGM simulations we used the 140 ka BP combined ice sheet reconstruction (Tarasov et al., 2012; Abe-Ouchi et al., 2013; Briggs et al., 2014) detailed in the PGM PMIP4 protocol (Menviel et al., 2019). Vegetation is prescribed based on a pre-industrial distribution and kept constant. As ice cover changes, the fractions of grid cells that are land ice versus other surface types changes proportionally, altering albedo. However, since there is no dynamical vegetation component, some important climate-ice-vegetation feedbacks are neglected which could have a significant impact on ice sheet evolution (Stone and Lunt, 2013). Sea Surface Temperature (SST) and sea ice concentration is also prescribed and constant and is taken from HadCM3 simulations of 21 ka BP and 140 ka BP (Figs. B1 and B2). The modelled annual average SSTs are cooler at the LGM than at the PGM, everywhere, except in the North Atlantic due to less sea ice cover in this region (Fig. 2b). However, the summer SSTs are warmer in the NH at the LGM compared to the PGM. The decision to use these constant SST and sea ice fields, rather than a statistical reconstruction as in Gandy et al., (2023), was made due to the lack of both empirical and modelled PGM SST data available to produce an equivalent reconstruction. The HadCM3 SSTs are colder on average than the reconstruction in Gandy et al., (2023), with the largest differences, of up to 6 ºC, seen in the tropics and mid-latitudes. This may introduce another source of uncertainty in the simulations. In the ice sheet model, we use the same ice sheet domain and initial condition for the LGM and PGM, which is the same as used in Gandy et al., (2023). The interactive ice sheet model domain in Glimmer covers North America and Greenland, and the initial ice sheet extent, thickness and bedrock elevation is from a previous Last Deglaciation ensemble of the NAIS, at 18.2 ka BP (Gregoire et al., 2016). This is a smaller intermediate

https://doi.org/10.5194/cp-2024-10
Preprint. Discussion started: 12 February 2024

(MIS 3 like) ice sheet which is used as an approximate pre-glacial maximum extent from which to grow the ice sheet towards an equilibrium ice volume.

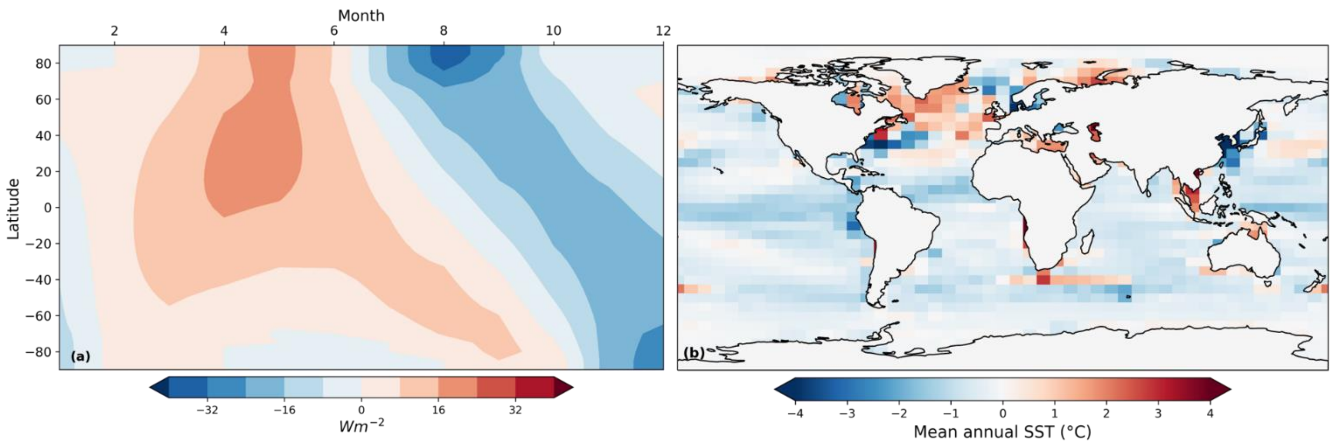

Figure 2. Difference between the LGM and PGM (a) latitudinal distribution of incoming top of the atmosphere shortwave radiation each month, and (b) modelled sea surface temperatures.

2.3 Ensemble design

The ensemble by Gandy et al., (2023) showed that uncertainty in parameters controlling SMB, ice sheet dynamics and climatic conditions over the ice sheets had a significant influence on the extent and volume of the LGM NAIS, with albedo parameters explaining the majority of the variation in model output. Since these parameters needed re-tuning from simulations of the present day Greenland ice sheet to produce an acceptable LGM NAIS configuration in FAMOUS-ice, the PGM may also show different sensitivities to the uncertain parameters. Therefore, we run new ensembles of the LGM and PGM in order to quantify uncertainties and identify combinations of climate and ice sheet parameters that perform well for both periods.

Following on from Gandy et al., (2023), a second wave of simulations was performed and compared to reconstructions of ice sheet extent and volume to identify NROY parameter combinations (see methodology in Appendix C), the results of which formed the basis of the ensemble design in this study. We reran the LGM ensemble to allow for slight changes in the experiment design compared to Gandy et al., (2023): we use orbital parameters for 21 ka BP rather than 23 ka BP and HadCM3 SSTs instead of a reconstruction (see Sect. 2.2). Table 2 details the 13 parameters that were varied in these simulations. Out of the 176 NROY parameter combinations from the Wave 2, a representative subset of 62 were selected which provided adequate coverage of the NROY space (see Appendix C for details). Each was run for 1000 climate years (10,000 ice sheet years) for both the LGM and PGM set ups until the majority of the ice sheet has reached close to equilibrium. Despite differences in the model set up between this study and Gandy et al., (2023), we expect the 62 samples chosen from their design to be a good estimate to an optimal parameter design for our set up (Appendix C).

https://doi.org/10.5194/cp-2024-10
Preprint. Discussion started: 12 February 2024

Table 2. Description of parameters varied in the ensembles. Adapted from Gandy et al., (2023).

Parameter	***Description***
Lapse Rate	Prescribed lapse rate for air temperature used to downscale FAMOUS near-surface ice sheet climate onto surface elevation tiles. Downwelling longwave radiation is also adjusted for consistency.
Daice	Sensitivity of bare-ice albedo to surface air temperatures once the surface is in a melt regime.
Rho	The threshold in surface snow density at which the FAMOUS albedo scheme switches from a scattering paradigm appropriate for a conglomeration of snow grains to one more appropriate for a solid surface.
AV_GR	Sensitivity of the snow albedo to variation in surface grain size.
RHcrit	The threshold of relative humidity for cloud formation (R. Smith, 1990). A higher value means clouds can form less easily.
VF1	The precipitating ice fall-out speed (Heymsfield, 1977).
CT	The conversion rate of cloud liquid water droplets to precipitation (R. Smith, 1990).
CW	The threshold values of cloud liquid water for formation of precipitation (R. Smith, 1990). Only the value for the land is varied.
Entrainment Coefficient	Convection Scales rate of mixing between environmental air and convective plume.
Alpham	The sea ice low albedo (Crossley & Roberts, 1995).
Basal Sliding	The basal sliding rate. A higher value allows increased ice velocity.
Mantle Relaxation Time	The relaxation time of the mantle, a lower value essentially making the mantle less viscous, thus allowing a quicker topographic rebound.
Flow Enhancement Factor	The softness of ice. Increasing the factor makes the ice softer and more deformable (Rutt et al., 2009).

https://doi.org/10.5194/cp-2024-10
Preprint. Discussion started: 12 February 2024

3 Results and discussion

3.1 Ensembles

3.1.1. Unconstrained ensembles

Our ensembles of 62 North American Ice Sheet configurations spans uncertainty in model parameters and reveals the wide range of possible modelled ice sheet evolutions. Over the full ensembles, we find that the set-up of the original Wave 2 meant that the albedo values were too high and so the use of more realistic albedos in these ensembles led to many of the runs deglaciating to very low volumes as shown in Fig. 3 (see Appendix C for more detail).

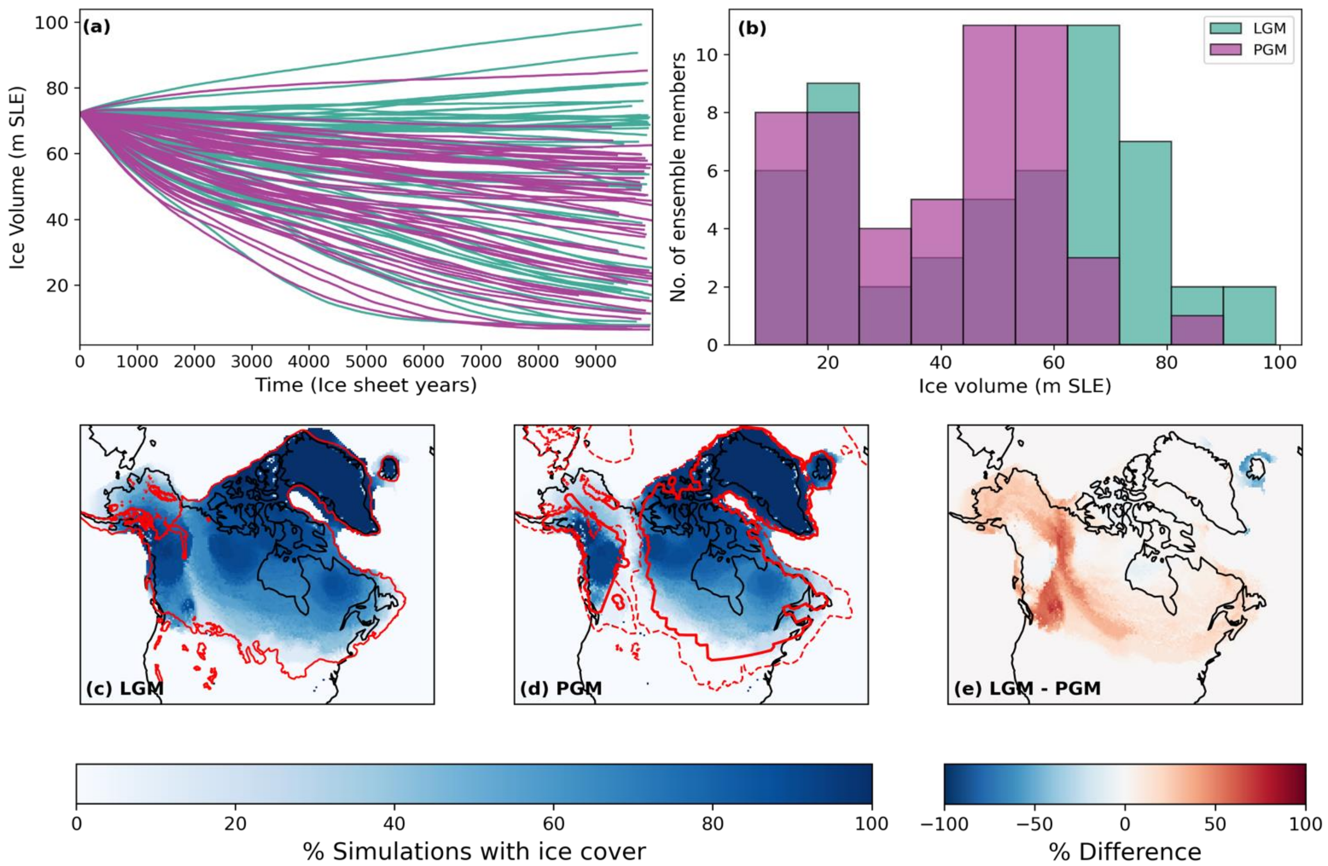

Figure 3. (a) Ice volume evolution over modelled time, and (b) density distribution of final ice volumes for the full LGM and PGM ensembles. Percentage of simulations with ice cover for (c) LGM (with the Dalton et al., (2020) reconstructed margin shown in red); (d) PGM (with the PMIP4 PGM modelled margin shown in solid red and the Batchelor et al., (2019) reconstructed maximum MIS 6 margin shown in dashed red), and (e) the difference between the LGM and PGM, at the end of the simulations.

https://doi.org/10.5194/cp-2024-10
Preprint. Discussion started: 12 February 2024

3.1.2. Constrained ensembles

To filter out implausible ice sheet configurations in the results, a set of constraints, based on southern ice sheet extent and volume, were applied to the LGM ensemble. Both ensembles were filtered based on the LGM results since the extent of the NAIS is very well constrained by geological data and there are more estimates of ice volume for the LGM than the PGM. This is because there is a lack of empirical data (over both space and time) on ice sheet configuration at the PGM due to destruction by subsequent glaciations and difficulties with dating what is available (Parker et al., 2022). Thus, most of the reconstructions of NAIS extent for this period are actually the maximum extent over the whole of MIS 6 (190-132 ka BP) and are mostly based on numerical modelling combined with this scarce proxy data (e.g. Colleoni et al., 2016; Batchelor et al., 2019). The NROY LGM results can then be compared to the corresponding PGM results to advance understanding of the differences that occurred and reveal whether parameters that performed well for the LGM also give plausible PGM results. Ice extent was assessed against the reconstruction by Dalton et al. (2020). We focus our evaluation of ice extent on the southern NAIS area and chose to disregard regions of known model bias. This includes marine margins that are subject to processes not included in Glimmer and the Alaskan regions where small climate model biases lead to ice sheet overgrowth (e.g. Ganopolski et al., 2010; Gregoire et al. 2016, Sherriff-Tadano et al., 2023). Additionally, ice lobes are not well captured in many models so we do not expect our simulations to perfectly match the reconstructed Southern NAIS extent. To account for this, we applied a tolerance on the Southern ice sheet area of 1.79 x 10^6 km^2, equivalent to 3 times the area of the lobes (Fig. 4). We thus calculate the Southern NAIS ice area as the integrated area within the large box shown in Fig. 4 at the end of each LGM simulation and selected simulations that matched the reconstructed area from Dalton et al. (2020) within plus or minus 1.79 x 10^6 km^2. The volume of the NAIS is not as well constrained by proxy data and so estimates rely on ice sheet, glacial isostatic adjustment and sea level modelling studies. Based on a number of these studies, a minimum NAIS (including Greenland) volume of 70 m SLE (2.8 x 10^7 km^3) was applied to the ensemble (Marshall et al., 2002; Tarasov and Peltier, 2002; 2004; Tarasov et al., 2012; Lambeck et al., 2014; Peltier et al., 2015; Rohling et al., 2017; Batchelor et al., 2019; Gowan et al., 2021). The volumes in meters sea level equivalent are calculated based on present day ocean area.

https://doi.org/10.5194/cp-2024-10
Preprint. Discussion started: 12 February 2024

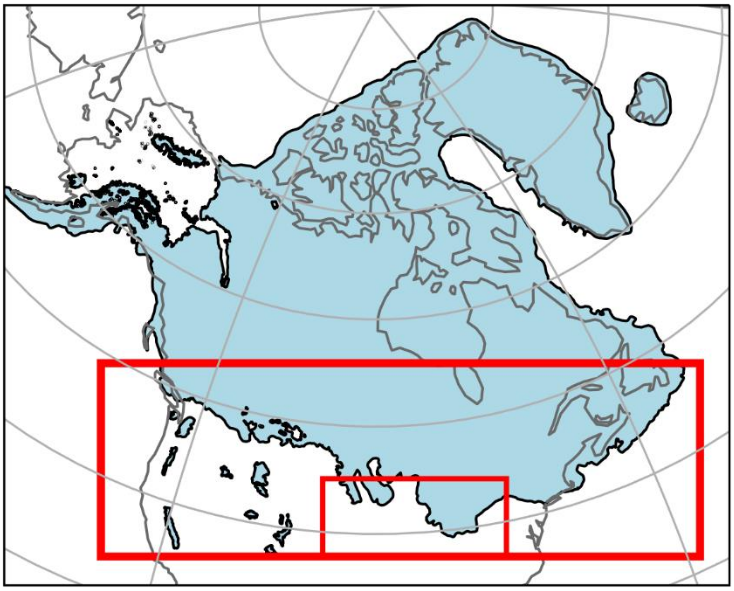

Figure 4. Outline of the LGM North American Ice Sheet by Dalton et al. (2020). The large red box shows the region we use to calculate reconstructed and modelled Southern NAIS area. The small red box shows the region used to calculate the area of the lobes for setting as the upper and lower target bounds.

Table 3. Average volumes (NAIS + Greenland) and southern NAIS areas and their standard deviations (SD) of the NROY LGM and PGM simulations. Also shown are estimated values from literature for comparison.

	Mean Total Volume (SD), m SLE	*Estimated Total Volume, m SLE*	*Mean Southern Area (SD), x 10^6 km^2*	*Estimated Southern Area, x 10^6 km^2*
LGM	82.1 (8.29)	61-98 (Rohling et al., 2017)	5.55 (0.33)	6.28 (Dalton et al., 2020)
PGM	62.3 (10.3)	49-69 (Rohling et al., 2017)	3.64 (0.82)	3.32 (Menviel et al., 2019)

After applying our metric constraints, six non-implausible or NROY LGM simulations remained. Table 3 gives the average volumes and areas of these six simulations and the corresponding six PGM ice sheets compared to estimated values from empirical and model data. All six LGM simulations show an overgrowth of ice in Alaska of varying magnitudes, as a result of the previously mentioned climate model bias. However, in other regions the simulations display a very similar ice extent, with the southern area only varying by 9.7 x 10^5 km^2. None of the simulations form ice lobes as expected but show a close match to reconstructed ice extent in our target area and in the marine regions (Fig. 6a). There is a minimum ice volume of 73.9 m

https://doi.org/10.5194/cp-2024-10
Preprint. Discussion started: 12 February 2024

SLE and a maximum of 97.1 m SLE. The maximum ice thickness varies by around 300 m but the overall shapes of the ice sheets remain the same, with the thickest ice towards the east of the ice sheet over Hudson Bay.

All the PGM ice sheets were smaller in volume than their LGM counterpart (Figs. 5 and 6) and displayed a smaller extent in the southern margin and the saddle region between the western Cordilleran Ice Sheet and eastern Laurentide Ice Sheet. However, the PGM simulations also displayed more variability in their ice extent and volumes. The ice volumes range from 53.4 m SLE to 83.37 m SLE and the southern extent varies by 2.44 x 10^6 km^2. The range in maximum ice thickness is also over double the LGM, varying by around 613 m. These PGM configurations also look plausible compared to the less well constrained extent data available, including previous empirical and modelled reconstructions of the PGM/MIS 6 extent (Menviel et al., 2019; Batchelor et al., 2019; Fig. 6b). For example, all the simulations maintain an ice-free corridor between the Laurentide and Cordilleran ice sheets which is a common feature in these PGM reconstructions. In addition, the excess Alaskan ice seen in LGM simulations is also present at the PGM, however the growth is not as excessive. We therefore conclude that in our model, based on the available empirical constraints, parameters that produce a good LGM NAIS also produce a plausible PGM NAIS using PGM boundary and initial conditions (orbital parameters, SSTs and orography). Our simulations can thus be compared and analysed to understand the causes of the different configurations between the two periods.

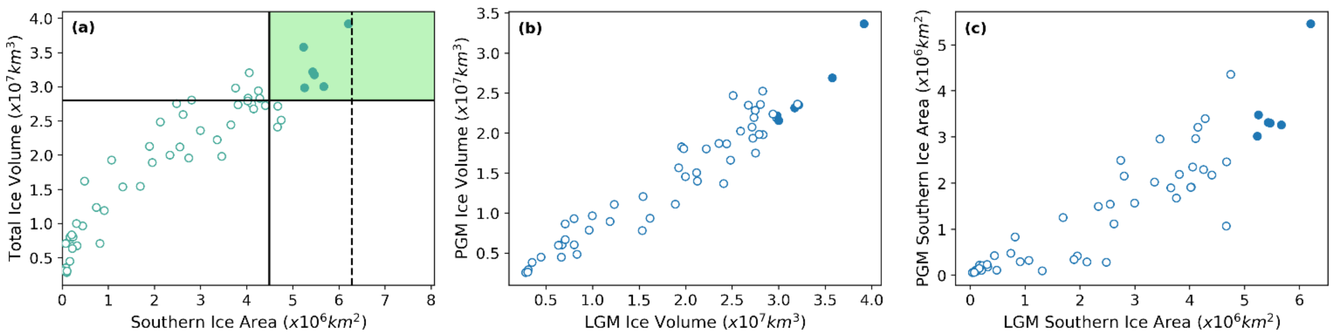

Figure 5. (a) The relationship between final ice volume and southern area for the LGM ensemble, and the relationship between the LGM and PGM; (b) final ice volume, and (c) final southern areas. The filled in blue dots represent the six NROY LGM simulations and the solid lines on panel (a) show the minimum volume and area constraints applied to the ensemble.

https://doi.org/10.5194/cp-2024-10
Preprint. Discussion started: 12 February 2024

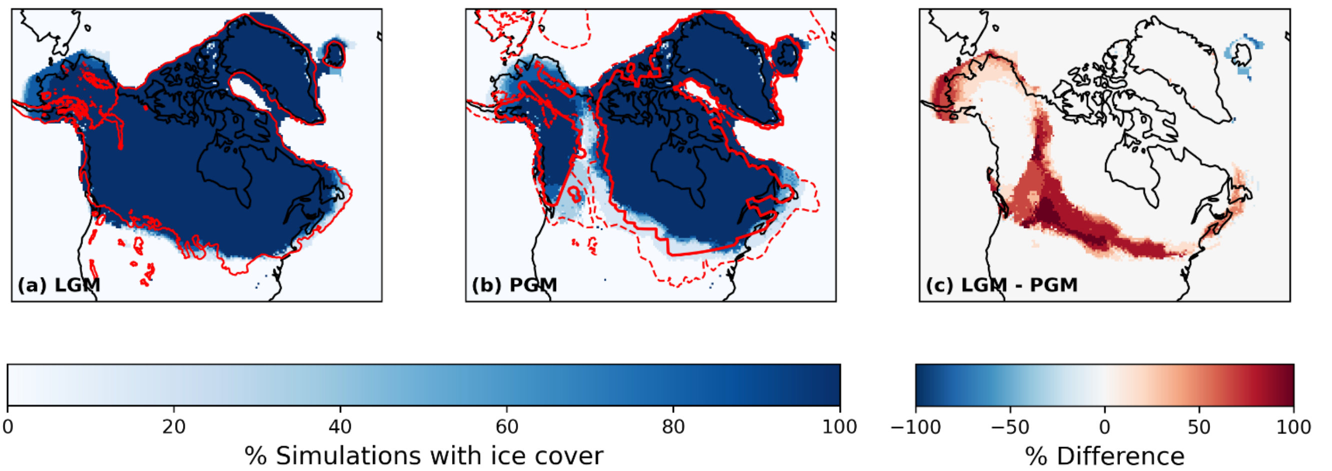

Figure 6. Percentage of simulations with ice cover for (a) LGM with the Dalton et al., (2020) reconstructed margin shown in red; (b) PGM with the PMIP PGM modelled margin shown in solid red and the Batchelor et al., (2019) reconstructed maximum MIS 6 margin shown in dashed red, and (c) the difference between the LGM and PGM, at the end of the simulations for the six NROY ensemble members.

3.2 Uncertainty due to model parameters

Most of the uncertainty in the results for both the LGM and PGM can be explained by parameters that affect the surface albedo of the ice sheet (*Daice, Rho* and *AV_GR*) and *basal sliding* (Fig. 7). Similar conclusions were drawn by Gandy et al., (2023), on which this study is based, as well as other ensemble based studies exploring the sensitivity of the LGM NAIS to model parameters (e.g. Sherriff-Tadano et al., 2023). The similar behaviour between the LGM and PGM across the parameter ranges (Figs. D1 and D2) further implies that similar model parameter values are appropriate for use when modelling both periods and within the bounds of available model and data constraints, our results show that retuning the model would not lead to significant changes in predicted ice sheet configurations between the LGM and PGM. . However, since the ice volume is most sensitive to surface albedo and most simulations deglaciate under low values of *Daice*, this suggests that the value of bare ice albedo in the model may need to be increased for future work.

Additionally, the difference in ice volume and area between the LGM and PGM is most influenced by the parameters *AV_GR*, *Daice* and *basal sliding*, however the effect of these parameters on the differences seen is minor (Fig. D3). This suggests that the higher the albedo and lower the ice sheet velocity, the more sensitive the ice sheet is to changes in radiative forcings from the orbital boundary conditions. Due to the sampling strategy, this ensemble is not the best design to analyse the sensitivity of the ice sheets during the two time periods to the different parameters and would require a larger ensemble and a sensitivity analysis with Gaussian Process emulation (e.g. Pollard et al., 2023), as is presented in Gandy et al. (2023) and Sherriff-Tadano et al. (2023).

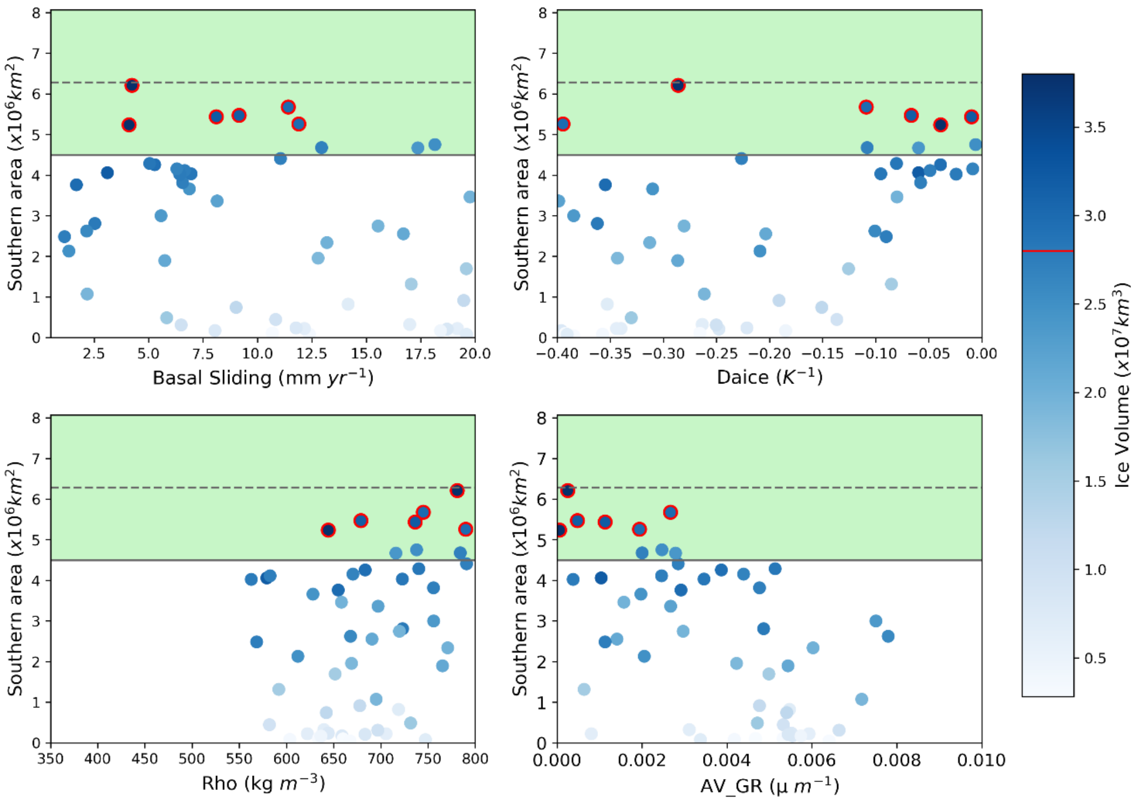

Figure 7. Relationship between LGM southern area and the four most influential parameters. The green shaded region shows the southern area constraint applied with the dotted line showing the exact area of the reconstruction and the solid line the minimum bound applied. The colour scale represents ice volume and the dots outlined in red are the six NROY LGM simulations with the red line on the colour bar showing the volume constraint.

3.3 Climate-ice sheet interactions

The main cause of the difference in configurations between the LGM and PGM in this study is the less negative SMB at the LGM in the saddle region (Fig. 8). This is mostly a result of much lower ablation rates (runoff) in the summer months (JJA) at the LGM compared to the PGM, and to a lesser extent in spring and autumn (MAM and SON), and an increase in sublimation. The accumulation (snowfall) is similar between the two periods and does not contribute much to the SMB difference.

https://doi.org/10.5194/cp-2024-10
Preprint. Discussion started: 12 February 2024

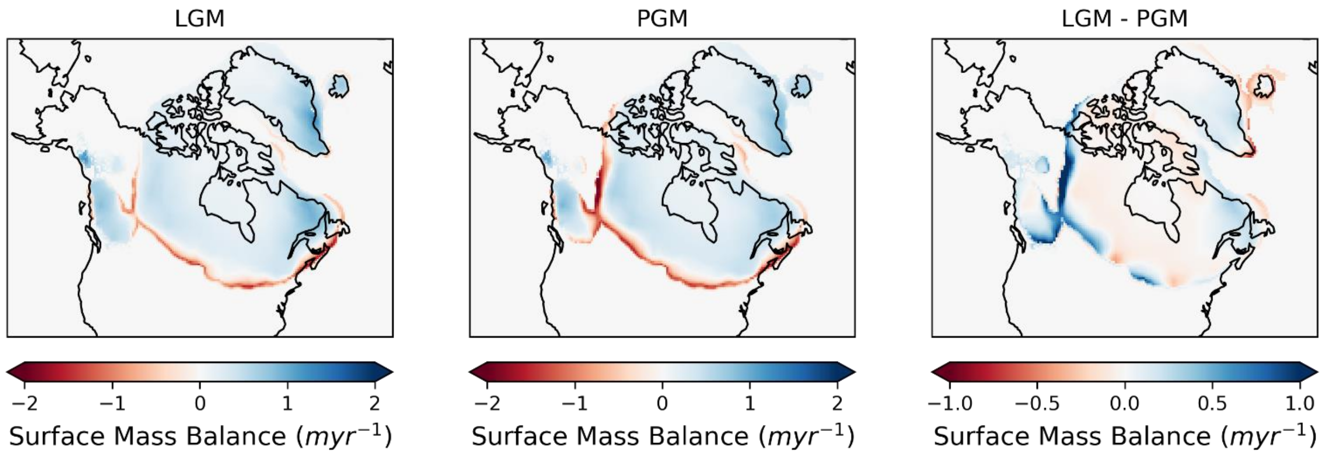

Figure 8. Mean surface mass balance of the constrained LGM and PGM ensembles averaged over model years 10 - 20 of the simulations and the difference between them.

This reduction in runoff occurs despite the LGM receiving more incoming top of the atmosphere shortwave radiation in early summer and more incoming surface radiation over North America at this time (Fig. 9a). Therefore, the positive SMB anomaly is a result of much more of this shortwave radiation being reflected back off the surface causing lower surface temperatures than at the PGM, allowing ice to build up and be maintained. In other words, the LGM has a higher albedo in this saddle region resulting in a more positive ice-albedo feedback (Figs. 9b and 9c). In contrast, the PGM has much lower albedo over the southern margin and saddle region, preventing ice growth in these regions.

During the analysis of these runs, we found that the coupling in the model was not passing all reductions in ice sheet area from Glimmer to FAMOUS in certain regions, particularly where entire FAMOUS gridboxes were initially covered in ice at all elevations (i.e. the saddle region at the LGM). This would have tended to reinforce the initial high albedo, positive mass balance surface conditions in the saddle region for the LGM configuration but would not have prevented the PGM simulations from growing ice in that area. To assess the role played by the initial conditions in our model simulations, we present an additional sensitivity analysis in the following section.

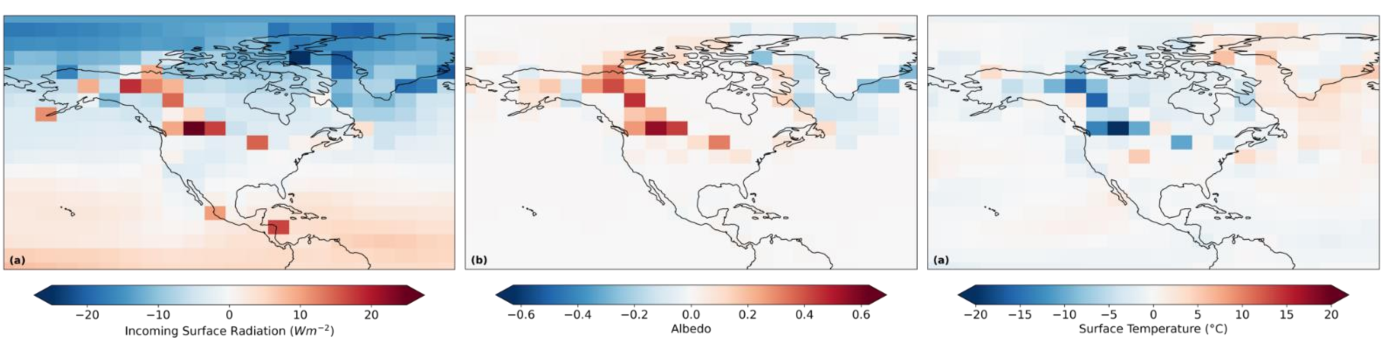

https://doi.org/10.5194/cp-2024-10
Preprint. Discussion started: 12 February 2024

Figure 9. Mean difference between the NROY LGM and PGM simulations of mean summer (a) incoming surface shortwave radiation; (b) albedo, and (c) surface temperature. All plots show the June-July-August average over model years 10-20 of the simulations.

3.4 Sensitivity analysis

To investigate the sensitivity of the final ice volumes to these differences in the initial conditions versus the differences in the climate, a sensitivity analysis was carried out along with factorisation based on the method used in Lunt et al., (2012), also used in Gregoire et al. (2015). We divided the differences in inputs between LGM and PGM into two factors; the initial ice sheet configuration used in FAMOUS and the climate boundary conditions (orbital parameters, greenhouse gases and SSTs/sea ice). Thus, the total difference in final ice volume (ΔV) between the LGM and the PGM can be written as Eq. (1):

$$\Delta \mathrm{V} = \mathrm{d}V_{ice} + dV_{climate} \,, \tag{1}$$

where dV_{ice} is the difference in final ice volume due to the different initial ice sheet configurations and $dV_{climate}$ is the difference due to the difference climate boundary conditions used.

The factorisation method requires 2^N simulations (where N is the number of different components) to determine the contribution of each component to ice volume difference, therefore $2^2 = 4$ experiments are needed that systematically change one variable. These experiments are listed in Table 4. We chose one of the NROY pairs of simulations (xpken and xpkyn respectively) to carry out this analysis, these thus correspond to the full LGM and PGM simulations (E and E_{ci} respectively) in the factorial decomposition. We further performed the two additional simulations needed for the decomposition (Table 4). The relative contributions of the initial conditions and climate can be calculated by Eqs. (2) and (3):

$$dV_{ice} = \frac{1}{2}\big((V_i - V) + (V_{ci} - V_c)\big), \tag{2}$$

$$dV_{climate} = \frac{1}{2}\big((V_c - V) + (V_{ci} - V_i)\big), \tag{3}$$

Table 4. Ice sheet and climate conditions in each of the four experiments used in the sensitivity analysis

Experiment (final volume)	***FAMOUS initial ice sheet***	***Climate (PMIP4)***
E (V)	LGM GLAC1D	LGM
E_c (V_c)	LGM GLAC1D	PGM
E_i (V_i)	PGM PMIP4	LGM
E_{ci} (V_{ci})	PGM PMIP4	PGM

https://doi.org/10.5194/cp-2024-10
Preprint. Discussion started: 12 February 2024

The results show that between the LGM and the PGM there was a total volume decrease (dV_1) of 8.89 x 10^6 km^3. The initial ice sheet configuration (dV_{i1}) alone caused a decrease of 1.12 x 10^7 km^3 (125% contribution) but this was offset by the climatic conditions (dV_{c1}) which resulted in an increase in volume of 2.27 x 10^6 km^3 (25% contribution) (Figs. 10a-c). To further understand the effect of initial conditions, we performed further simulations in which the initial conditions in the ice sheet component Glimmer was set to closely match the initial ice sheet extent and topography set in the climate component FAMOUS. Specifically, for the LGM, the Glimmer initial bedrock topography and ice surface elevation was prescribed from the GLAC-1D reconstruction used in the FAMOUS LGM boundary condition. For the PGM, the data needed for PMIP4 reconstruction to be converted to the Glimmer initial condition were not available. Instead, both Glimmer and FAMOUS were initialised with the final timestep of the PGM experiment (xpkyn) since it closely resembles the PMIP4 reconstruction. This produced a similar result to the original factorial decomposition, with the initial ice conditions (dV_{i2}) resulting in a 35% decrease in volume which was offset by the climate (dV_{c2}) by a 4% increase (Figs. 10d-f).

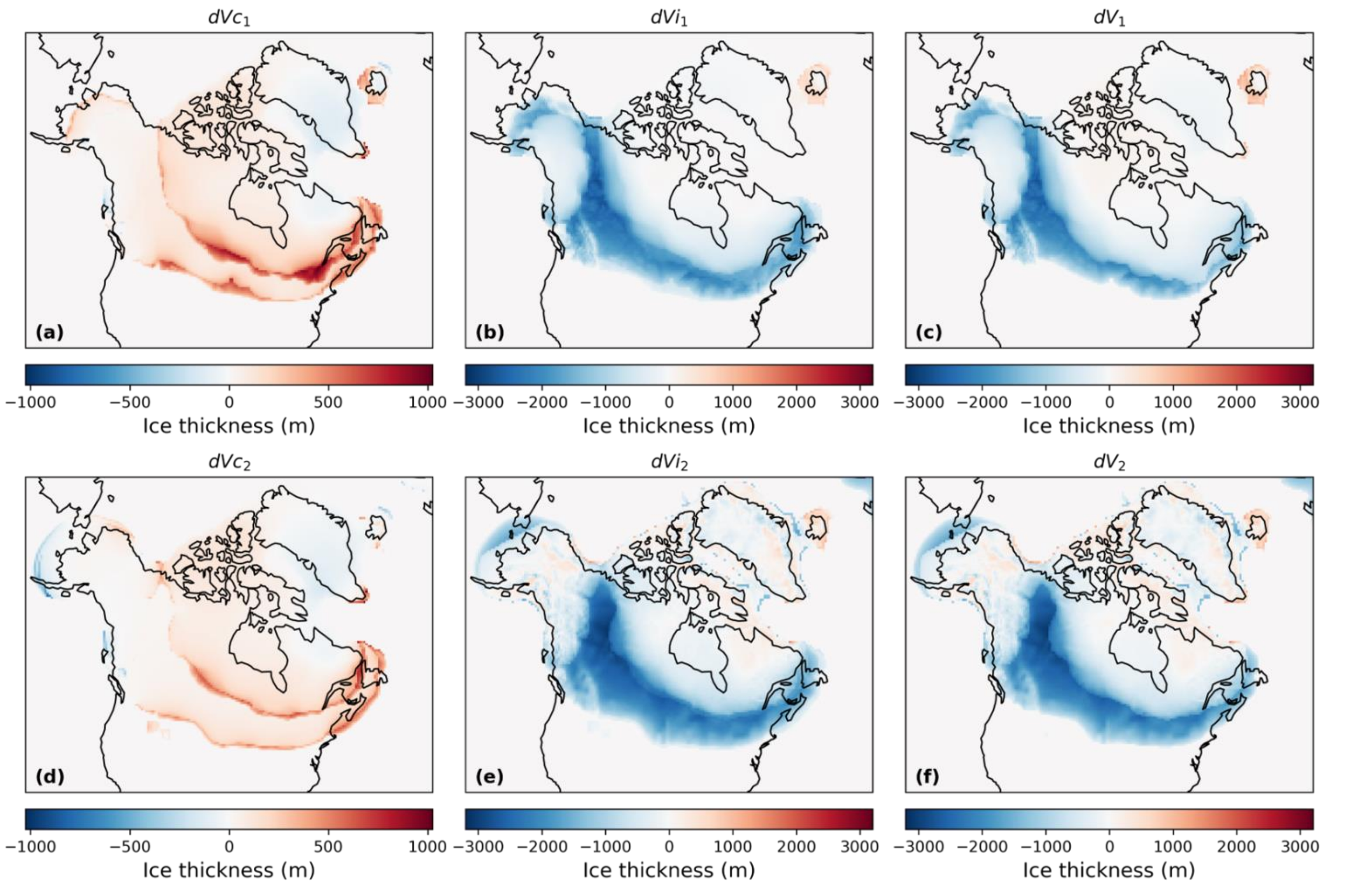

Figure 10. Difference in final ice thickness between the PGM and LGM due to (a) climate parameters; (b) initial ice sheet conditions, and (c) the total difference. (d-f) show the same but for the corrected Glimmer ice sheets.

https://doi.org/10.5194/cp-2024-10
Preprint. Discussion started: 12 February 2024

Based on these results, it is clear that the difference in initial ice cover, and resulting ice-albedo feedback, overwhelmingly determined the difference in final ice volume between the LGM and PGM in these simulations. Additionally, the vegetation fraction in the non-ice covered areas in the PGM initial conditions will have a compounding effect on this difference by introducing a vegetation-albedo feedback that limits the ice growth at the PGM. A similar conclusion was obtained by Abe-Ouchi et al., (2007) who studied the relative contribution to climate over ice sheets from the ice sheet itself and the orbital parameters and CO_2 concentration. They found the cooling caused by the ice sheet themselves was the dominant effect, mostly due to albedo feedbacks, which increase with ice sheet area. Kageyama et al., (2004) also highlighted in their study the importance of the albedo feedback on the maximum modelled North American ice volume. They show that changes in vegetation are needed to initiate glaciation over North America which is then accelerated by the ice-albedo feedback.

Interestingly, the difference in orbital parameters, GHGs and SSTs (climate) between the LGM and PGM caused a larger North American ice sheet at the PGM in contrast to what evidence suggests. This is mostly a result of the orbital configuration which resulted in the Northern Hemisphere receiving less incoming solar radiation in spring and early summer (Table 1; Fig 2). This reduces the melting of snow that has accumulated in winter. The winter snow accumulation is also higher at the PGM than the LGM due to warmer air temperatures in autumn and winter, as a result of the orbital configuration, leading to a wetter climate. Summer SSTs are also cooler at the PGM due to lower spring insolation, further contributing to reduced runoff. In contrast, the Greenland ice sheet decreases in size due to PGM climate conditions likely due to higher sea ice concentration south of Greenland reducing the moisture source available for precipitation (Fig. 2b). This result highlights the importance of the evolution of these climate factors and the ice sheets during the preceding glacial cycles in determining the glacial maxima configurations.

For example, during the start of the Last Glacial Cycle (MIS 5; ~115-80 ka BP), the variation in 65º N summer insolation was relatively large as a result of changes in orbital parameters (Fig 11a-c), which resulted in multiple cycles of growth and recession of the North American Ice Sheets during this period, but total ice volume remained low (Bonelli et al., 2009; Ganopolski et al., 2010; Dalton et al., 2022). Insolation then reaches a minimum at ~70 ka BP (Fig 11c) which, combined with decreasing concentrations of CO_2 (~190 ppm at ~65 ka BP; Fig. 11f), lead to a significant increase in ice sheet volume to almost LGM extent (Fig. 11d) and a switch to more widespread glacial conditions at the MIS 5/MIS 4 transition (Bonelli et al., 2009; Dalton et al., 2022). The size of the NAIS at this time was large enough to induce positive feedbacks, such as the ice-albedo feedback, allowing its maintenance throughout MIS 4 and MIS 3 (~70-30 ka BP) despite an increase in insolation from ~50-30 ka BP (Fig. 11c). This was also supported by a continued decrease in CO_2 (Bonelli et al., 2009). Growth of the ice sheet could then continue to its glacial maximum extent following a further insolation and CO_2 decrease during MIS 2 (~30-21 ka BP) (Fig. 11c-f). In contrast, prior to the PGM there were peaks in insolation at ~172 and ~148 ka BP that reached higher levels than were reached during MIS 4 and MIS 2, respectively, which were significant periods of growth at the LGM (Fig. 11i; Berger; 1978). This may have inhibited an initial significant build-up of ice over North America, as during MIS 4, preventing the initiation of an ice-albedo feedback strong enough to enable the continued growth towards a larger LGM

https://doi.org/10.5194/cp-2024-10
Preprint. Discussion started: 12 February 2024

configuration and/or maintain its volume through the second insolation peak. In addition, there was more time between the LGM and the insolation maximum at ~50-30 ka BP compared to the PGM and the maximum at ~147 ka BP. Therefore, the PGM NAIS may have not had enough time to regrow before insolation started to increase again.

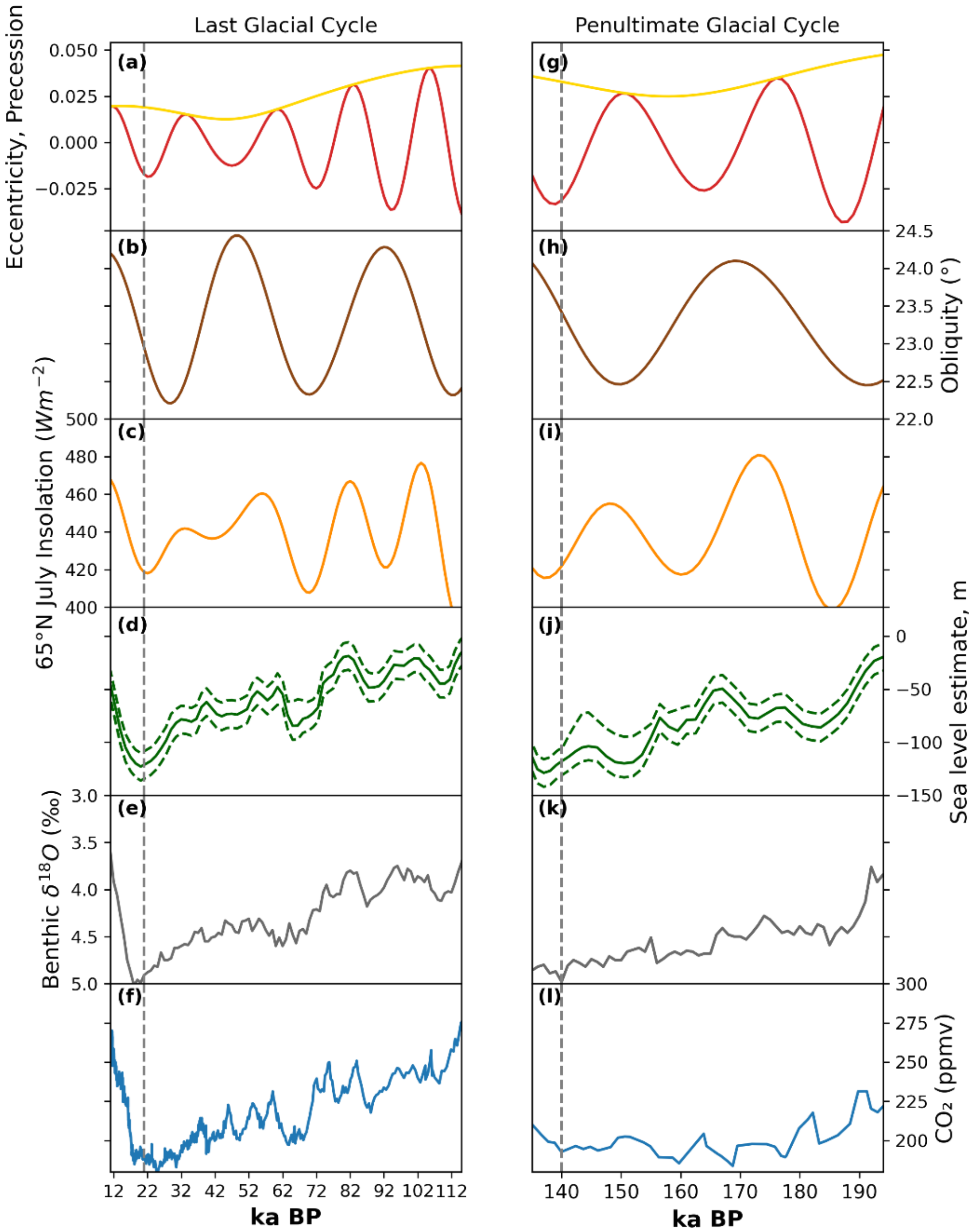

https://doi.org/10.5194/cp-2024-10
Preprint. Discussion started: 12 February 2024

Figure 11. Evolution of climate proxies over the last two glacials: (a,g) precession index (red) with eccentricity as an envelope (yellow); (b,h) obliquity (Berger, 1978); (c,i) July insolation at 65° N (Berger and Loutre, 1999); (d,j) reconstruction of global mean sea level and uncertainty estimate (dotted lines) (Waelbroeck et al., 2002); (e,k) benthic δ18O global stack record (Lisiecki and Raymo, 2005), and (f,l) EPICA Dome C carbon dioxide ice core records (Luthi et al., 2008; Bereiter et al., 2015). The PGM and LGM are indicated by the dotted line.

4 Conclusions

We have performed and compared ensemble simulations of the LGM and the PGM using a coupled climate-ice sheet model (FAMOUS-ice) with an interactive North American Ice Sheet. The model was able to successfully simulate the ice sheet at both periods, compared to empirical evidence and other modelling studies, under different LGM and PGM climate boundary conditions and initial ice sheets. Overall, this study has shown that the underlying surface conditions, ice and snow cover and vegetation, used as boundary conditions in coupled climate-ice sheet simulations are extremely important in the resulting ice sheet volumes and extents because of the strong influence of the ice-albedo and vegetation-albedo feedbacks on the expansion of ice. In this study, the climate of each glacial maxima period has only a negligible effect on the simulated ice volume. Thus, investigation of the processes and interactions that took place prior to the glacial maxima will be needed to fully understand why the LGM and PGM NAIS configuration differed.

Additional feedbacks that played a role in the development of glacials into either an LGM-like or PGM-like mode are also missing in these simulations due to computational constraints. For example, the low resolution of the atmospheric component of FAMOUS means that it is capable of performing ensembles and long paleo runs while directly coupled to an ice sheet model, however it also means that many small-scale atmospheric processes (e.g. stationary wave response) caused by and affecting the ice sheet topography are not captured (Kageyama and Valdes, 2000; Liakka and Nilsson, 2010; Beghin et al., 2014; 2015; Liakka et al., 2012; 2016). Additionally, the shallow ice approximation used in Glimmer means that the ice sheet will not be able to simulate marine instabilities of advance and retreat (Pattyn et al., 2012). This effect will be minimal for the NAIS, but a more advanced ice sheet model would be required to simulate a marine ice sheet like the EIS.

As previously mentioned, the vegetation was kept fixed at present day distributions but the vegetation prior to and next to the ice cover has been shown to be very important for determining ice sheet expansion in models through the vegetation-albedo feedback (Kageyama et al., 2004; Colleoni et al., 2009b; Horton et al., 2010; Stone and Lunt, 2013). Therefore, implementing glacial maxima distributions or dynamical vegetation may affect the results since the reduction in forest and expansion of tundra/shrubs compared to present day would increase the albedo of the surface next to the ice and affect the climate (Meissner et al., 2003). Similarly, the fixed SSTs and sea ice concentrations used introduce uncertainty due to lack of constraint data and neglect any effects changes in ocean conditions and ice sheets have on each other (e.g. Timmerman et al., 2010; Colleoni et al., 2011; Ullman et al., 2014; Sherriff-Tadano et al., 2018; 2021). We recommend the use of a fully coupled atmosphere-ocean-vegetation-ice sheet model to further investigate these feedbacks. The effect of dust deposition and ice dammed lakes have also been shown to have a large influence on the build-up of ice (e.g. Krinner et al., 2004; 2006; Naafs et al., 2012; Colleoni et al., 2009a) however further model developments would be needed to investigate these effects.

Finally, the Eurasian ice sheet also displayed important differences between the LGM and PGM and had a large influence on the climate. It is likely that some of the differences in the configurations of the NAIS and EIS between the two glacial maxima resulted from their interactions with each other (Beghin et al., 2014; 2015; Liakka et al., 2016). To investigate the EIS at the PGM, we recommend the use of an efficient marine ice sheet model such as BISICLES that uses Adaptive Mesh Refinement to refine the processes occurring at marine margins that are more important for the marine based Eurasian ice sheet (Cornford et al., 2013; Gandy et al., 2019).

Appendix A: Eccentricity equation correction

The equation for the role of eccentricity on solar insolation used in the simulations in this paper was:

$$S(t) = S_o\left(1+\frac{e^2}{2}\right)(1+e\cos v)/(1-e^2))^2 \quad (4)$$

However, this is incorrect and has now been corrected in the model to:

$$S(t) = S_o((1+e\cos v)/(1-e^2))^2 \quad (5)$$

The PGM experiment 'xpky0' was re-run with the correct equation and shows that on average the SMB was slightly more negative in our simulations than it should have been, leading to slightly smaller ice sheets (Fig. A1). However, the impact is small (and would be even smaller for the LGM given the lower eccentricity) and does not affect our overall conclusions.

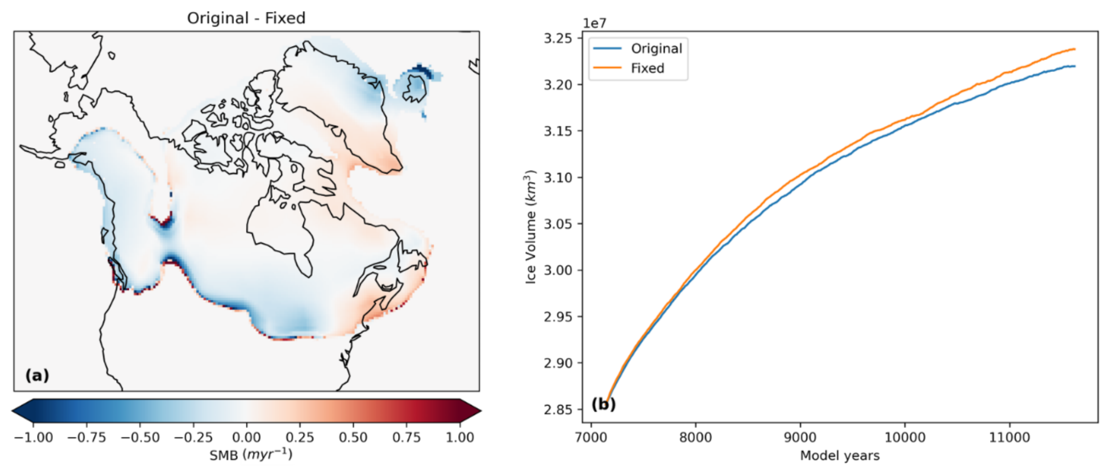

Figure A1. (a) Difference between the SMB after 450 model years between the original simulation and the simulation using the corrected eccentricity equation and (b) the evolution of ice sheet volume for both experiments.

https://doi.org/10.5194/cp-2024-10
Preprint. Discussion started: 12 February 2024

Appendix B: Sea surface temperatures

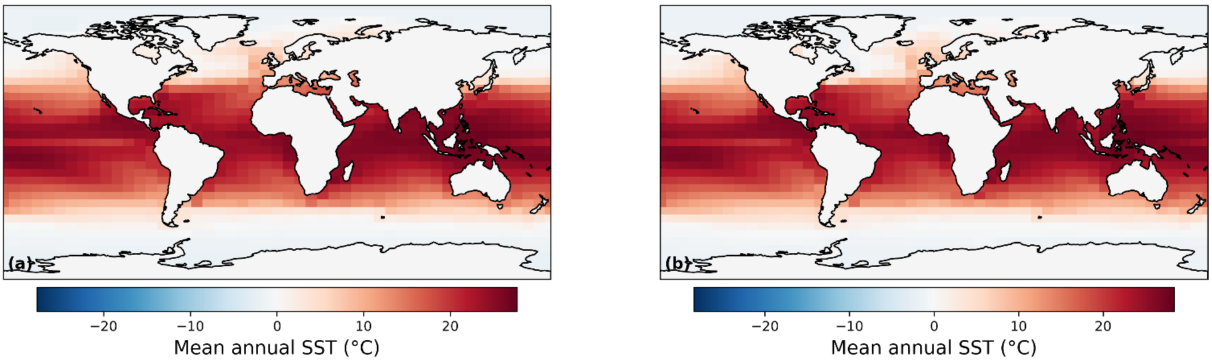

Figure B1. Mean annual SSTs used in this study from HadCM3 for (a) LGM and (b) PGM.

Appendix C: Wave 2 methodology

The ensemble design in this study was based on the 'Not Ruled Out Yet' (NROY) parameter combinations from a second wave of ensemble members that followed on from the 280 member ensemble performed in Gandy et al., (2023). From the first wave of simulations, only 18 out of these 280 members produced a large enough LGM North American Ice sheet to meet the volume and extent criteria they imposed (see details in reference). Further work was thus performed to augment the ensemble of simulations that met the NROY criteria. We used statistical emulation to identify plausible regions in the parameter space. As there was limited information to constrain the domain of plausibility in the parameter space, we instead implemented an early-stopping criteria that allowed us to prevent the full execution of model runs that were not expected to produce good ice sheets. To do this we first modelled, from Wave 1, the predicted equilibrium area of the ice sheet from the value of the initial surface mass balance. Mathematically, we specified;

$$A = f(b) + \epsilon, \qquad (6)$$

where A is the 'equilibrium' ice sheet area after 10,000 ice sheet years, b is the 20 year averaged SMB value and $f(\cdot)$ may be any function. We considered f to be either linear or sampled from a Gaussian Process (GP) and found the linear model gave more conservative uncertainty estimates which was desired since the Wave 2 runs needed to bound the NROY space. The predictive interval for the model is $P(b) = [f(b) + 3\sqrt{\mathrm{var}(\epsilon)}, f(b) - 3\sqrt{\mathrm{var}(\epsilon)}]$ and we targeted equilibrium ice sheet areas in the interval $T = [1.5\times10^7\ \mathrm{km}^2, 2\times10^7\ \mathrm{km}^2]$. The interval T is analogous to the target interval defined using Pukelsheim's 3-sigma rule in standard history matching (Pukelsheim, 1994). Plausible values of b satisfy the condition that $P(b) \cap T$ is non-zero, that is, for b to be plausible, the predictive bound $P(b)$ and the plausible equilibrium ice sheet area T must intersect. It was found that the 20-year averaged SMB had to be at least positive to produce a plausible ice sheet.

https://doi.org/10.5194/cp-2024-10
Preprint. Discussion started: 12 February 2024

To further improve efficiency, we used statistical emulation to produce plausible values of b (and hence equilibrium ice sheet areas); iterating the training data of the emulator with each wave of simulator runs. Define by $\boldsymbol{x}$ the multivariate vector of parameters that they build the emulator over: here $\boldsymbol{x}$ comprised of the 4 most influential parameters *Fsnow*, *AV_GR*, *Daice*, and *Flow Factor*. We model b with a random error process, $b \sim GP(x) + \eta$, where the effects of the parameters not explicitly represented in $\boldsymbol{x}$ are handled by the stochasticity of the process represented by η. Values of b were sampled using a stratified k-extended Latin Hypercube design (Williamson, 2015) and three sub-waves were executed, from which, a candidate set for the Wave 2 ensemble was extracted.

The first sub-wave (Wave 1.1) samples 200 ensemble members, which are predicted from the emulator to have non-negligible probability of positive SMB. This results in around 50% of simulations in this sub-wave having a positive SMB, an increase from 15% in the original wave (Fig. C1, Wave 1.1). We attempt to refine the predictive bounds on the GP model twice more (Fig. C1, Wave 1.2 and 1.3), with no improvement. This is likely due to the inherent stochasticity of the climate model and cumulative effects of the parameters that they absorb into the predictive error term. At the end of this process of iterative short waves, the candidate set contains over 1000 20-year long simulations that have a positive SMB over the North American ice sheet. From this candidate set, and again using stratified k-extended Latin Hypercubes, we select an optimal (with respect to space-filling and accounting for the previous Wave 1 runs) design of 200 ensemble members to continue for a full 10,000 years to an equilibrium North American Ice Sheet. These 200 simulations make up the Wave 2. For context, this workflow of GP model sub-waves saved around 230,000 core hours (or about two months of real time) compared to running a full second ensemble wave.

Out of these 200 Wave 2 simulations, 176 members were identified to be NROY based on the original volume and extent thresholds. It is based on these results that we sub-sampled 62 parameter combinations for our simulations. This number of simulations was selected to enable us to run long equilibrium LGM and PGM simulations over a full ensemble within reasonable computational requirements. From the 176 NROY parameter combinations we randomly generated 10^7 candidate designs of size 62 from which we selected an approximate maximin design. This is obtained by: first linearly transforming each parameter onto the same range of [0, 1] to aid comparability; before computing the minimum distance between a parameter vector and its nearest neighbour; and then selecting the candidate design that maximised this distance. The resulting design possesses parameter vectors which are well-spaced and thus adequately cover the NROY space.

Our simulations use slightly different orbital parameter values and sea surface conditions to that of Gandy et al., (2023) (see Sect. 2). Thus, we do not expect the sample of 62 parameter combinations to provide full coverage of the NROY space but, as seen in section S2 of the supplementary information in Gandy et al., (2023), the output trends are sufficiently similar that we expect this to be close enough to an optimal sample. Whilst we may have also sampled some parameter combinations outside of the NROY space, we feel these will still provide valuable information about uncertainty in outputs at the LGM and PGM. Our detailed comparison to observations (see Sect. 3.1) identified six parameter combinations that match our criteria for LGM

https://doi.org/10.5194/cp-2024-10
Preprint. Discussion started: 12 February 2024

and PGM ice extent and volume, thus demonstrating the success of this approach. Further exploration of the parameter space may produce NROY simulations in a different part of the parameter space but would not change the conclusion of this paper. Upon analysing the results, we found a technical error in the original Wave 2 ensemble which resulted in the values of the parameter *Daice* being shifted from its intended range of –0.4-0 K^{-1} to 0-0.4 K^{-1}, this means that the albedo of the bare ice was increasing with melting, which is likely not the case. This produced larger values of surface albedo and thus larger ice sheets in these Wave 2 simulations (not shown here). In the ensemble of simulations presented here, we corrected the *Daice* values to match the intended parameter range. In some simulations, the switch of *Daice* value from a large positive number to a large negative number would have resulted in a decrease in surface albedo and resulting ice sheet volume. This effect is negligible for values of *Daice* closer to zero.

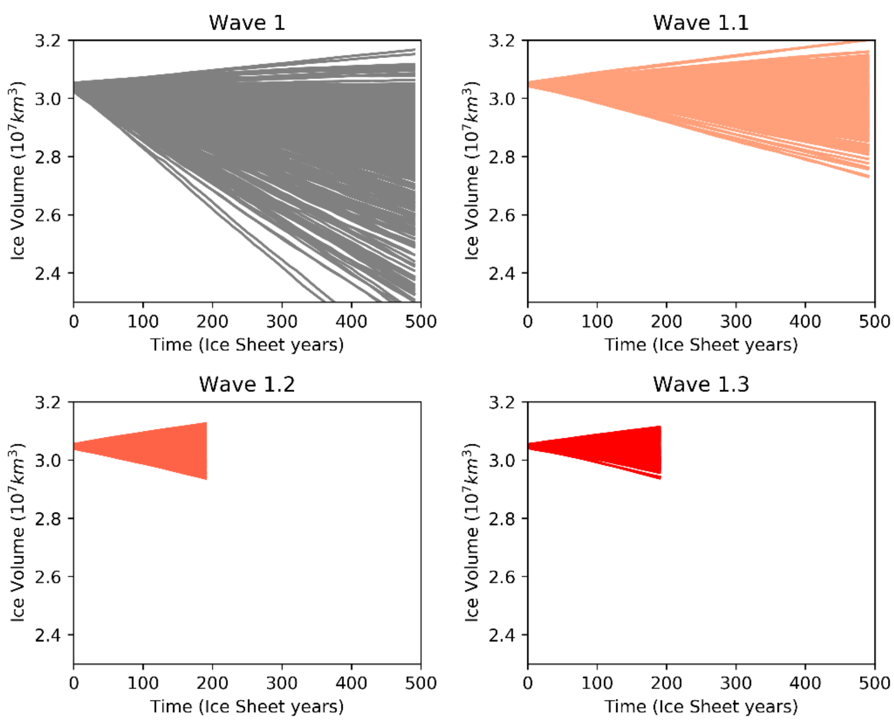

Figure C1. Ice volumes simulated in the successive ensemble sub-waves of simulations sampled to have a positive initial surface mass balance using the Gaussian Process emulator

Appendix D: Metrics vs parameters plots

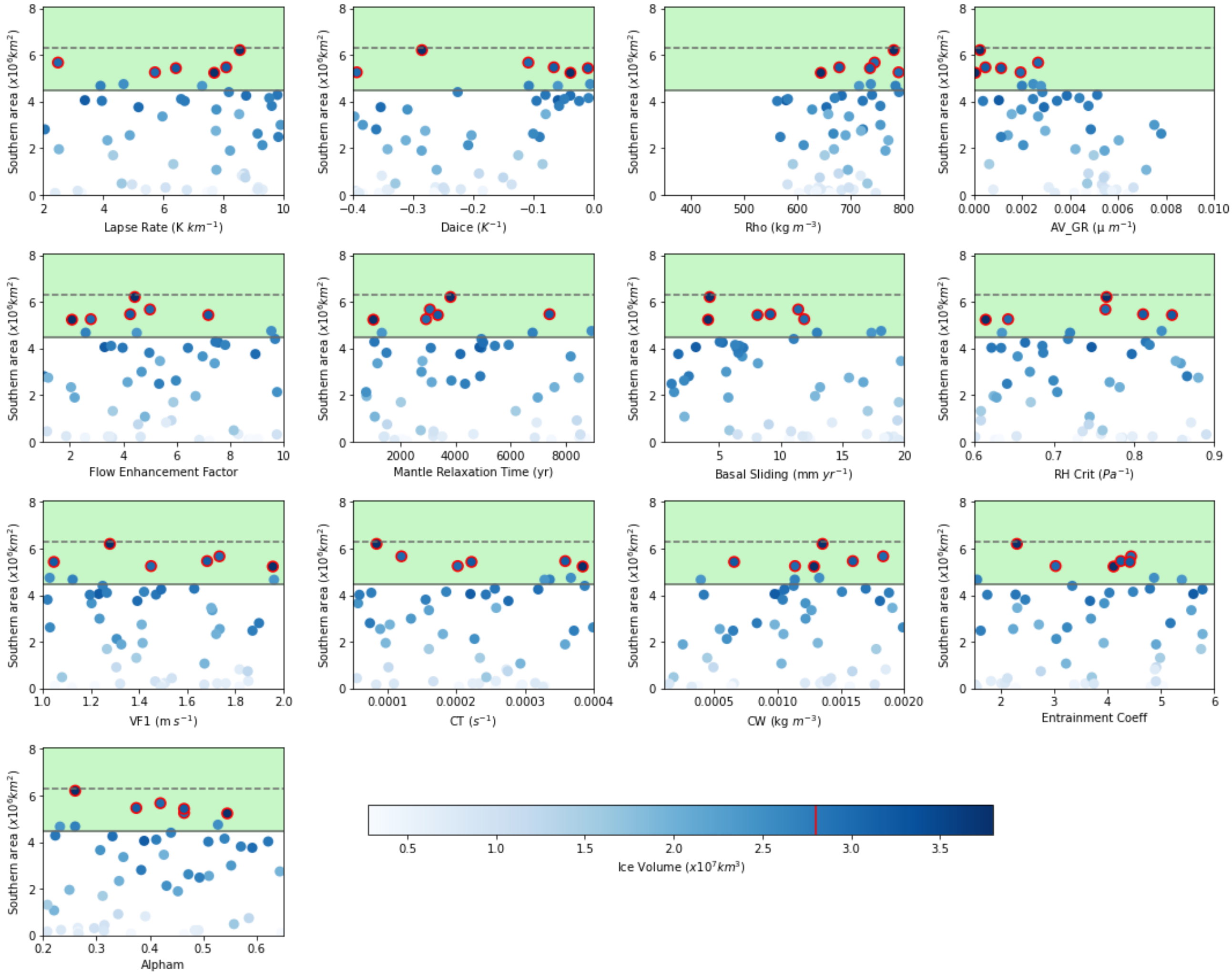

Figure D1. Southern area versus each of the 13 parameters varied for the LGM ensemble. The green shaded region shows the southern area constraint applied with the dotted line showing the exact area of the reconstruction and the solid line the solid line the minimum bound applied. The colour scale represents ice volume and the dots outlined in red are the six NROY LGM simulations with the red line on the colour bar showing the volume constraint.

https://doi.org/10.5194/cp-2024-10
Preprint. Discussion started: 12 February 2024

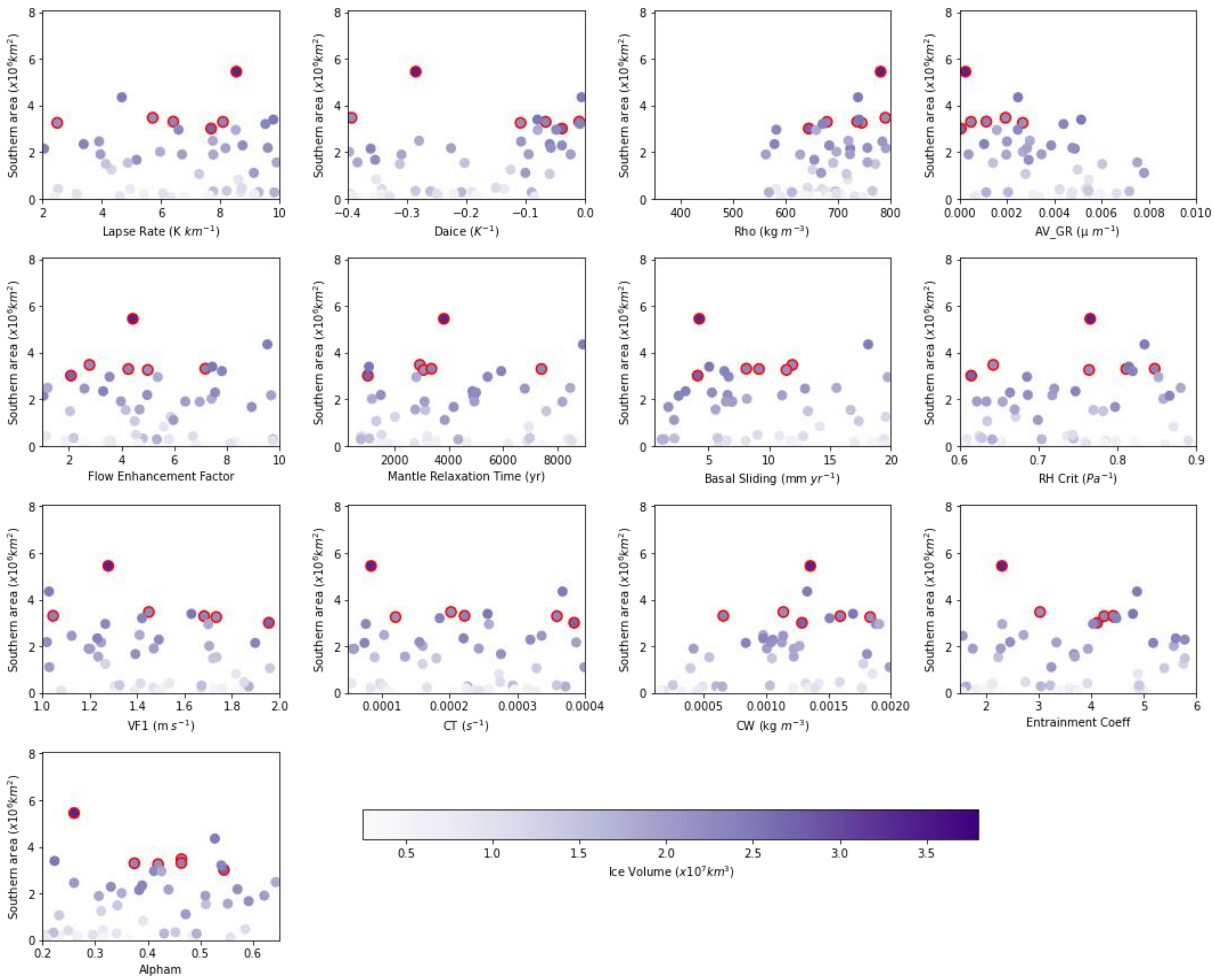

Figure D2. Southern area versus each of the 13 parameters varied for the PGM ensemble. The colour scale represents ice volume and the dots outlined in red are the corresponding six NROY PGM simulations.

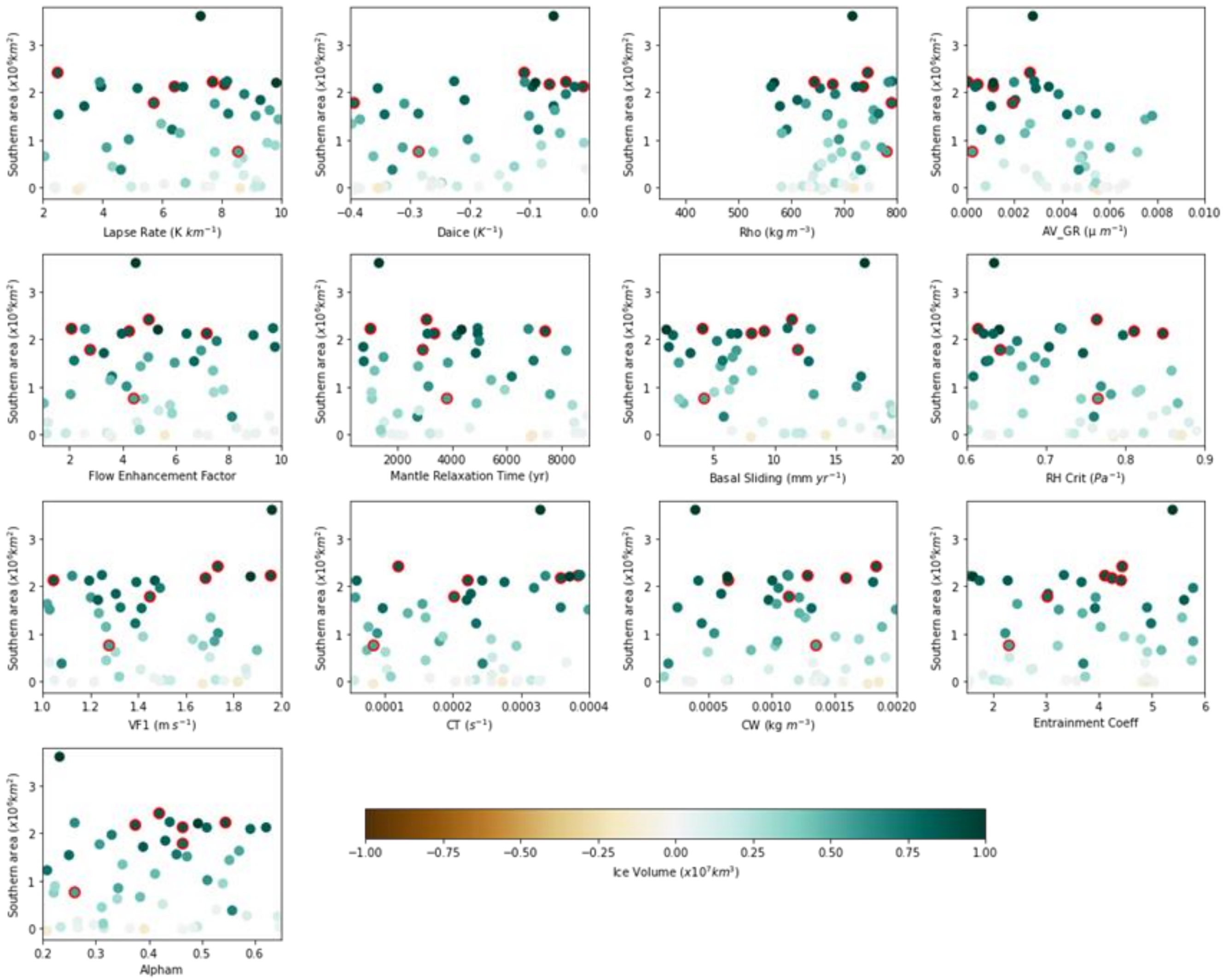

Figure D3. Difference in southern area versus each of the 13 parameters varied between the LGM and PGM ensemble members. The colour scale represents difference in ice volume and the dots outlined in red are the six NROY simulations.

https://doi.org/10.5194/cp-2024-10
Preprint. Discussion started: 12 February 2024

Data availability

For this pre-print, the boundary conditions used in this study as well as the full ensemble ice sheet model output and volume and extent metrics, climate timeseries for the NROY simulations and final ice volume data from the sensitivity tests have been made available to reviewers. All other model output data are available on request.

Author contributions

VLP lead the project and performed the majority of the work. VLP, LJG, RFI and NG designed the simulations and VLP and NG prepared the initial and boundary conditions with support from OGP. VLP ran the simulations and analysed the results. LCA and NG designed and performed the Wave 2 simulations the ensembles were sampled from, and JO did the sampling. RSS provided technical support and updates for FAMOUS-Glimmer. VLP wrote the manuscript with comments and contributions from all co-authors. LJG, RFI and NG supervised the project and LJG acquired the funding.

Competing interests

The authors declare they have no conflict of interest.

Acknowledgements

This research is primarily funded by the ‘SMB-Gen’ UKRI Future Leaders Fellowship MR/S016961/1, with LJG and JO directly supported by the award and VLP’s PhD studentship funded by the University of Leeds. RFI and RSS’s contributions were supported by the RISICMAP19 NERC standard grant NE/T007443/1. LCA is supported by the ARC ITRH for Transforming energy Infrastructure through Digital Engineering (TIDE), Grant No. IH200100009. OGP is funded by the European Union’s Horizon 2020 research and innovation programme (grant agreement no. 802281). The simulations were run on the high-performance research computing facilities of the University of Leeds and technical support was provided by Richard Rigby from the Centre for Environmental Modelling and Computation (CEMAC). The authors would like to thank Paul Valdes for providing the HadCM3 LGM and PGM sea surface temperature and sea ice datasets. Also, Michel Crucifix, Peter Hopcroft, Pam Vervoort and Paul Valdes for discovering the eccentricity equation error and providing the corrected equation.

References

Abe-Ouchi, A., Segawa, T., and Saito, F: Climatic Conditions for modelling the Northern Hemisphere ice sheets throughout the ice age cycle, Clim. Past, 3, 423–438, https://doi.org/10.5194/cp-3-423-2007, 2007.

Abe-Ouchi, A., Saito, F., Kawamura, K., Raymo, M. E., Okuno, J., Takahashi, K., and Blatter, H.: Insolation-driven 100,000-year glacial cycles and hysteresis of ice-sheet volume, Nature, 500, 190-193, https://doi.org/10.1038/nature12374, 2013.

Batchelor, C. L., Margold, M., Krapp, M., Murton, D. K., Dalton, A. S., Gibbard, P. L., Stokes, C. R., Murton, J. B., and Manica, A.: The configuration of Northern Hemisphere ice sheets through the Quaternary, Nat. Commun., 10, 3713, https://doi.org/10.1038/s41467-019-11601-2, 2019.

Beghin, P., Charbit, S., Dumas, C., Kageyama, M., Roche, D. M., and Ritz, C.: Interdependence of the growth of the Northern Hemisphere ice sheets during the last glaciation: the role of atmospheric circulation, Clim. Past, 10, 345–358, https://doi.org/10.5194/cp-10-345-2014, 2014.

Beghin, P., Charbit, S., Dumas, C., Kageyama, M., and Ritz, C.: How might the North American ice sheet influence the northwestern Eurasian climate?, Clim. Past, 11, 1467–1490, https://doi.org/10.5194/CP-11-1467-2015, 2015.

Bereiter, B., Eggleston, S., Schmitt, J., Nehrbass-Ahles, C., Stocker, T. F., Fischer, H., Kipfstuhl, S., and Chappellaz, J.: Revision of the EPICA Dome C CO_2 record from 800 to 600-kyr before present, Geophys. Res. Lett., 42, 542–549, https://doi.org/10.1002/2014GL061957, 2015.

Berger, A. L.: Long-Term Variations of Daily Insolation and Quaternary Climatic Changes, J. Atmos. Sci., 35, 2362-2367, https://doi.org/10.1175/1520-0469(1978)035<2362:LTVODI>2.0.CO;2, 1978.

Berger, A., and Loutre, M. F.: Insolation values for the climate of the last 10 million years, Quaternary Sci. Rev., 10, 297–317, https://doi.org/10.1016/0277-3791(91)90033-Q, 1991.

Bonelli, S., Charbit, S., Kageyama, M., Woillez, M.-N., Ramstein, G., Dumas, C., and Quiquet, A.: Investigating the evolution of major Northern Hemisphere ice sheets during the last glacial-interglacial cycle, Clim. Past, 5, 329–345, https://doi.org/10.5194/cp-5-329-2009, 2009.

Briggs, R. D., Pollard, D., and Tarasov, L.: A data-constrained large ensemble analysis of Antarctic evolution since the Eemian, Quaternary Sci. Rev., 103, 91-115, https://doi.org/10.1016/j.quascirev.2014.09.003, 2014.

Cheng, H., Edwards, R. L., Broecker, W. S., Denton, G. H., Kong, X., Wang, Y., Zhang, R., and Wang, X.: Ice age terminations, Science, 326, 248–252. DOI: 10.1126/science.1177840, 2009.

Colleoni, F., Krinner, G., Jakobsson, M., Peyaud, V., and Ritz, C.: Influence of regional parameters on the surface mass balance of the Eurasian ice sheet during the peak Saalian (140 kya), Glob. Planet. Change, 68, 132-148, https://doi.org/10.1016/j.gloplacha.2009.03.021, 2009a.

Colleoni, F., Krinner, G., and Jakobsson, M.: Sensitivity of the Late Saalian (140 kyrs BP) and LGM (21 kyrs BP) Eurasian ice sheet surface mass balance to vegetation feedbacks, Geophys. Res. Lett., 36, L08704, doi:10.1029/2009GL037200, 2009b.

Colleoni, F., Liakka, J., Krinner, G., Jakobsson, M., Masina, S., and Peyaud, V.: The sensitivity of the Late Saalian (140 ka) and LGM (21 ka) Eurasian ice sheets to sea surface conditions, Clim. Dyn., 37, 531-553, https://doi.org/10.1007/s00382-010-0870-7, 2011.

Colleoni, F., Wekerle, C., Brandefelt, J., and Masina, S.: Constraint on the penultimate glacial maximum Northern Hemisphere ice topography (~140 kyrs BP), Quaternary Sci. Rev., 137, 97-112, https://doi.org/10.1016/j.quascirev.2016.01.024, 2016.

Cornford, S. L., Martin, D. F., Graves, D. T., Ranken, D. F., le Brocq, A. M., Gladstone, R. M., Payne, A. J., Ng, E. G., and Lipscomb, W. H.: Adaptive mesh, finite volume modeling of marine ice sheets, J. Comput. Phys., 232, 529–549, https://doi.org/10.1016/J.JCP.2012.08.037, 2013.

Crossley, J. F., and Roberts, D. L.: Thermodynamic/dynamic Sea-ice model, Meteorological office, 1995.

Dalton, A. S., Margold, M., Stokes, C. R., Tarasov, L., Dyke, A. S., Adams, R. S., Allard, S., Arends, H. E., Atkinson, N., Attig, J. W., Barnett, P. J., Barnett, R. L., Batterson, M., Bernatchez, P., Borns Jr, H. W., Breckenridge, A., Briner, J. P., Brouard, E., Campbell, J. E., Carlson, A. E., … Wright Jr, H. E.: An updated radiocarbon-based ice margin chronology for the last deglaciation of the North American Ice Sheet Complex, Quaternary Sci. Rev., 234, 106223, https://doi.org/10.1016/j.quascirev.2020.106223, 2020.

Dalton, A. S., Stokes, C. R., and Batchelor, C. L.: Evolution of the Laurentide and Innuitian ice sheets prior to the Last Glacial Maximum (115 ka to 25 ka), Earth-Sci. Rev., 224, 103875, https://doi.org/10.1016/j.earscirev.2021.103875, 2022.

Dentith, J. E., Ivanovic, R. F., Gregoire, L. J., Tindall, J. C., and Smith, R. S.: Ocean circulation drifts in multi-millennial climate simulations: the role of salinity corrections and climate feedbacks, Clim. Dyn., 52, 1761–1781, https://doi.org/10.1007/S00382-018-4243-Y/FIGURES/15, 2019.

Denton, G. H., Anderson, R. F., Toggweiler, J.R., Edwards, R. L., Schaefer, J. M., and Putnam, A. E.: The Last Glacial Termination, Science, 328, 1652-1656, DOI:10.1126/science.1184119, 2010.

Dutton, A., and Lambeck, K.: Ice Volume and Sea Level During the Last Interglacial, Science, 337, 216–219, https://doi.org/doi:10.1126/science.1205749, 2012.

Dutton, A., Carlson, A. E., Long, A. J., Milne, G. A., Clark, P. U., DeConto, R., Horton, B. P., Rahmstorf, S., and Raymo, M. E.: Sea-level rise due to polar ice-sheet mass loss during past warm periods, Science, 349, 6244, https://doi.org/10.1126/science.aaa4019, 2015.

Dyer, B., Austermann, J., D'Andrea, W. J., Creel, R. C., Sandstrom, M. R., Cashman, M., Rovere, A., and Raymo, M. E.: Sea-level trends across the Bahamas constrain peak last interglacial ice melt, Proc. Natl. Acad. Sci. U.S.A., 118, 33, https://doi.org/10.1073/pnas.2026839118, 2021.

Dyke, A.S., Andrews, J. T. Clark, P. U., England, J. H., Miller, G. H., Shaw, J., and Veillette, J. J.: The Laurentide and Innuitian ice sheets during the Last Glacial Maximum, Quaternary Sci. Rev., 21, 9-31, https://doi.org/10.1016/S0277-3791(01)00095-6, 2002.

Ehlers, J., Gibbard, P.L. and Hughes, P.D.: Chapter 4 – Quaternary Glaciations and Chronology, in: Past Glacial Environments, Second Edition, edited by: Menzies, J., and van der Meer, J.J.M., Elsevier, 77-101, https://doi.org/10.1016/B978-0-08-100524-8.00003-8, 2018.

Essery, R., Best, M., Betts, R., Cox, P. and Taylor, C.: Explicit Representation of Subgrid Heterogeneity in a GCM Land Surface Scheme, J. Hydrometeorol., 4, 530-543, https://doi.org/10.1175/1525-7541(2003)004<0530:EROSHI>2.0.CO;2., 2003.

Fyke, J. G., Weaver, A. J., Pollard, D., Eby, M., Carter, L., and Mackintosh, A.: A new coupled ice sheet/climate model: description and sensitivity to model physics under Eemian, Last Glacial Maximum, late Holocene and modern climate conditions, Geosci. Model Dev., 4, 117–136, https://doi.org/10.5194/gmd-4-117-2011, 2011.

Gandy, N., Gregoire, L. J., Ely, J. C., Cornford, S. L., Clark, C. D., and Hodgson, D. M.: Exploring the ingredients required to successfully model the placement, generation, and evolution of ice streams in the British-Irish Ice Sheet, Quaternary Sci. Rev., 223, 105915, https://doi.org/10.1016/j.quascirev.2019.105915, 2019.

Gandy, N., Astfalck, L. C., Gregoire, L. J., Ivanovic, R. F., Patterson, V. L., Sherriff-Tadano, S., Smith, R. S., Williamson, D., and Rigby, R.: De-tuning a coupled Climate Ice Sheet Model to simulate the North American Ice Sheet at the Last Glacial Maximum, J. Geophys. Res. Earth Surf.,, DOI: 10.1002/essoar.10512201.1, 2023.

Ganopolski, A., Calov, R., and Claussen, M.: Simulation of the last glacial cycle with a coupled climate ice-sheet model of intermediate complexity, Clim. Past, 6, 229–244, https://doi.org/10.5194/cp-6-229-2010, 2010.

Govin, A., Capron, E., Tzedakis, P. C., Verheyden, S., Ghaleb, B., Hillaire-Marcel, C., St-Onge, G., Stoner, J. S., Bassinot, F., Bazin, L., Blunier, T., Combourieu-Nebout, N., el Ouahabi, A., Genty, D., Gersonde, R., Jimenez-Amat, P., Landais, A., Martrat, B., Masson-Delmotte, V., … Zahn, R.: Sequence of events from the onset to the demise of the Last Interglacial: Evaluating strengths and limitations of chronologies used in climatic archives, Quaternary Sci. Rev., 129, 1–36, https://doi.org/10.1016/J.QUASCIREV.2015.09.018, 2015.

Gowan, E.J., Zhang, X., Khosravi, S., Rovere, A., Stocchi, P., Hughes, A. L. C., Gyllencreutz, R., Mangerud, J., Svendsen, J-I., and Lohmann, G.: A new global ice sheet reconstruction for the past 80 000 years, Nat. Commun., 12, 1199, https://doi.org/10.1038/s41467-021-21469-w, 2021.

Grant, K. M., Rohling, E. J., Bar-Matthews, M., Ayalon, A., Medina-Elizalde, M., Ramsey, C. B., Satow, C., and Roberts, A. P.: Rapid coupling between ice volume and polar temperature over the past 150,000 years, Nature, 491, 744-747. https://doi.org/10.1038/nature11593, 2012.

Gregoire, L., J. Modelling the Northern Hemisphere Climate and Ice Sheets during the Last Deglaciation, Ph.D. thesis, School of Geographical Sciences, University of Bristol, UK, 2010.

Gregoire, L., Payne, A. and Valdes, P.: Deglacial rapid sea level rises caused by ice-sheet saddle collapses, Nature, 487, 219–222, https://doi.org/10.1038/nature11257, 2012.

Gregoire, L. J., Valdes, P. J., and Payne, A. J.: The relative contribution of orbital forcing and greenhouse gases to the North American deglaciation, Geophys. Res. Lett., 42, 9970-9979, https://doi.org/10.1002/2015GL066005, 2015.

Gregoire, L. J., Otto-Bliesner, B., Valdes, P. J., and Ivanovic, R.: Abrupt Bølling warming and ice saddle collapse contributions to the Meltwater Pulse 1a rapid sea level rise, Geophys. Res. Lett., 43, 9130–9137, https://doi.org/10.1002/2016gl070356, 2016.

Gregoire, L. J., Ivanovic, R. F., Maycock, A. C., Valdes, P. J., and Stevenson, S.: Holocene lowering of the Laurentide ice sheet affects North Atlantic gyre circulation and climate, Clim. Dyn., 51, 3797-3813, https://doi.org/10.1007/s00382-018-4111-9, 2018.

Gregory, J. M., Browne, O. J. H., Payne, A. J., Ridley, J. K., and Rutt, I. C.: Modelling large-scale ice-sheet–climate interactions following glacial inception, Clim. Past, 8, 1565–1580, https://doi.org/10.5194/cp-8-1565-2012, 2012.

Gregory, J. M., George, S. E., and Smith, R. S.: Large and irreversible future decline of the Greenland ice sheet, Cryosphere, 14, 4299–4322, https://doi.org/10.5194/TC-14-4299-2020, 2020.

Hemming, S. R.: Heinrich events: Massive late Pleistocene detritus layers of the North Atlantic and their global climate imprint, Rev. Geophys., 42, RG1005, https://doi.org/10.1029/2003RG000128, 2004.

Horton, D., Poulsen, C. and Pollard, D.: Influence of high-latitude vegetation feedbacks on late Palaeozoic glacial cycles, Nat. Geosci., 3, 572–577, https://doi.org/10.1038/ngeo922, 2010.

Huybers, P.: Early Pleistocene Glacial Cycles and the Integrated Summer Insolation Forcing, Science, 313, 508-511, DOI:10.1126/science.1125249, 2006.

Ivanovic, R. F., Gregoire, L. J., Kageyama, M., Roche, D. M., Valdes, P. J., Burke, A., Drummond, R., Peltier, W. R., and Tarasov, L.: Transient climate simulations of the deglaciation 21–9 thousand years before present (version 1) – PMIP4 Core experiment design and boundary conditions, Geosci. Model Dev., 9, 2563–2587, https://doi.org/10.5194/gmd-9-2563-2016, 2016.

Ivanovic, R. F., Gregoire, L. J., Burke, A., Wickert, A. D., Valdes, P. J., Ng, H. C., Robinson, L. F., McManus, J. F., Mitrovica, J. X., Lee, L., and Dentith, J. E.: Acceleration of Northern Ice Sheet Melt Induces AMOC Slowdown and Northern Cooling in Simulations of the Early Last Deglaciation, Paleoceanogr. Paleoclimatol., 33, 807–824, https://doi.org/10.1029/2017PA003308, 2018.

Izumi, K., Valdes, P., Ivanovic, R., and Gregoire, L.: Impacts of the PMIP4 ice sheets on Northern Hemisphere climate during the last glacial period, Clim. Dyn., 60, 2481-2499, https://doi.org/10.1007/s00382-022-06456-1, 2023.

Jiménez-Amat, P., and Zahn, R.: Offset timing of climate oscillations during the last two glacial-interglacial transitions connected with large-scale freshwater perturbation, Paleoceanography, 30, 768–788, https://doi.org/10.1002/2014PA002710, 2015.

Kageyama, M., and Valdes, P. J.: Impact of the North American ice-sheet orography on the Last Glacial Maximum eddies and snowfall, Geophys. Res. Lett., 27, 1515-1518, https://doi.org/10.1029/1999GL011274, 2000.

Kageyama, M., Charbit, S., Ritz, C., Khodri, M., and Ramstein, G.: Quantifying ice-sheet feedbacks during the last glacial inception, Geophys. Res. Lett., 31, 24, doi:10.1029/2004GL021339, 2004.

Kageyama, M., Albani, S., Braconnot, P., Harrison, S. P., Hopcroft, P. O., Ivanovic, R. F., Lambert, F., Marti, O., Peltier, W. R., Peterschmitt, J.-Y., Roche, D. M., Tarasov, L., Zhang, X., Brady, E. C., Haywood, A. M., Legrande, A. N., Lunt, D. J., Mahowald, N. M., Mikolajewicz, U., … Zheng, W.: The PMIP4 contribution to CMIP6-Part 4: Scientific objectives and experimental design of the PMIP4-CMIP6 Last Glacial Maximum experiments and PMIP4 sensitivity experiments, Geosci. Model Dev., 10, 4035–4055, https://doi.org/10.5194/gmd-10-4035-2017, 2017.

Kopp, R. E., Simons, F. J., Mitrovica, J. X., Maloof, A. C., and Oppenheimer, M.: Probabilistic assessment of sea level during the last interglacial stage, Nature, 462, 863-868, https://doi.org/10.1038/nature08686, 2009.

Krinner, G., Mangerud, J., Jakobsson, M., Crucifix, M., Ritz, C., and Svendsen, J-I.: Enhanced ice sheet growth in Eurasia owing to adjacent ice-dammed lakes, Nature, 427, 429–432, https://doi.org/10.1038/nature02233, 2004.

Krinner, G., Boucher, O., and Balkanski, Y.: Ice-free glacial northern Asia due to dust deposition on snow, Clim. Dyn., 27, 613–625, DOI:10.1007/s00382-006-0159-z, 2006.

Krinner, G., Diekmann, B., Colleoni, F., and Stauch, G.: Global, regional and local scale factors determining glaciation extent in Eastern Siberia over the last 140,000 years, Quaternary Sci. Rev., 30, 821-831, https://doi.org/10.1016/j.quascirev.2011.01.001, 2011.

Lambeck, K., Rouby, H., Purcell, A., Sun, Y., and Sambridge, M.: Sea level and global ice volumes from the Last Glacial Maximum to the Holocene, Proc. Natl. Acad. Sci. U.S.A., 111, 15296–15303, https://doi.org/10.1073/pnas.1411762111, 2014.

Landais, A., Dreyfus, G., Capron, E., Jouzel, J., Masson-Delmotte, V., Roche, D. M., Prié, F., Caillon, N., Chappellaz, J., Leuenberger, M., Lourantou, A., Parrenin, F., Raynaud, D., and Teste, G.: Two-phase change in CO_2, Antarctic temperature and global climate during Termination II. Nature Geoscience, 6, 1062–1065, https://doi.org/10.1038/ngeo1985, 2013.

Liakka, J., and Nilsson, J.: The impact of topographically forced stationary waves on local ice-sheet climate, J. Glaciol., 56, 534–544, https://doi.org/10.3189/002214310792447824, 2010.

Liakka, J., Nilsson, J. and Löfverström, M.: Interactions between stationary waves and ice sheets: linear versus nonlinear atmospheric response, Clim. Dyn., 38, 1249–1262, https://doi.org/10.1007/s00382-011-1004-6, 2012.

Liakka, J., Löfverström, M., and Colleoni, F.: The impact of the North American glacial topography on the evolution of the Eurasian ice sheet over the last glacial cycle, Clim. Past, 12, 1225–1241, https://doi.org/10.5194/CP-12-1225-2016, 2016.

Lisiecki, L. E., and Raymo, M. E.: A Pliocene-Pleistocene stack of 57 globally distributed benthic δ18O records, Paleoceanography, 20, 1–17, https://doi.org/10.1029/2004PA001071, 2005.

Loulergue, L., Schilt, A., Spahni, R., Masson-Delmotte, V., Blunier, T., Lemieux, B., Barnola, J. M., Raynaud, D., Stocker, T. F., and Chappellaz, J.: Orbital and millennial-scale features of atmospheric CH_4 over the past 800,000 years, Nature, 453, 383–386, https://doi.org/10.1038/nature06950, 2008.

https://doi.org/10.5194/cp-2024-10
Preprint. Discussion started: 12 February 2024

Lunt, D. J., Haywood, A. M., Schmidt, G. A., Salzmann, U., Valdes, P. J., Dowsett, H. J., and Loptson, C. A.: On the causes of mid-Pliocene warmth and polar amplification. Earth Planet. Sci. Lett., 321-322, 128-138, https://doi.org/10.1016/j.epsl.2011.12.042, 2012.

Lüthi, D., le Floch, M., Bereiter, B., Blunier, T., Barnola, J. M., Siegenthaler, U., Raynaud, D., Jouzel, J., Fischer, H., Kawamura, K., and Stocker, T. F.: High-resolution carbon dioxide concentration record 650,000–800,000 years before present, Nature, 453, 379–382. https://doi.org/10.1038/nature06949, 2008.

Margari, V., Skinner, L. C., Hodell, D. A., Martrat, B., Toucanne, S., Grimalt, J. O., Gibbard, P. L., Lunkka, J. P., and Tzedakis, P. C.: Land-ocean changes on orbital and millennial time scales and the penultimate glaciation, Geology, 4, 183–186, https://doi.org/10.1130/G35070.1, 2014.

Marino, G., Rohling, E. J., Rodríguez-Sanz, L., Grant, K. M., Heslop, D., Roberts, A. P., Stanford, J. D., and Yu, J.: Bipolar seesaw control on last interglacial sea level, Nature, 522, 197–201, https://doi.org/10.1038/nature14499, 2015.

Marshall, S. J., James, T. S., and Clarke, G. K. C.: North American Ice Sheet reconstructions at the Last Glacial Maximum, Quaternary Sci. Rev., 21, 175-192, https://doi.org/10.1016/S0277-3791(01)00089-0, 2002.

Masson-Delmotte, V., Stenni, B., Pol, K., Braconnot, P., Cattani, O., Falourd, S., Kageyama, M., Jouzel, J., Landais, A., Minster, B., Barnola, J. M., Chappellaz, J., Krinner, G., Johnsen, S., Röthlisberger, R., Hansen, J., Mikolajewicz, U., and Otto-Bliesner, B.: EPICA Dome C record of glacial and interglacial intensities, Quaternary Sci. Rev., 29, 113-128, https://doi.org/10.1016/j.quascirev.2009.09.030, 2010.

Meissner, K. J., Weaver, A. J., Matthews, H. D., and Cox, P. M.: The role of land surface dynamics in glacial inception: a study with the UVic Earth System Model, Clim. Dyn., 21, 515-537, https://doi.org/10.1007/s00382-003-0352-2, 2003.

Menviel, L., Capron, E., Govin, A., Dutton, A., Tarasov, L., Abe-Ouchi, A., Drysdale, R. N., Gibbard, P. L., Gregoire, L., He, F., Ivanovic, R. F., Kageyama, M., Kawamura, K., Landais, A., Otto-Bliesner, B. L., Oyabu, I., Tzedakis, P. C., Wolff, E., and Zhang, X.: The penultimate deglaciation: protocol for Paleoclimate Modelling Intercomparison Project (PMIP) phase 4 transient numerical simulations between 140 and 127 ka, version 1.0, Geosci. Model Dev., 12, 3649–3685, https://doi.org/10.5194/gmd-12-3649-2019, 2019.

Naafs, B. D. A., Hefter, J., Acton, G., Haug, G. H., Martinez-Garcia, A., Pancost, R., and Stein, R.: Strengthening of North American dust sources during the late Pliocene (2.7 Ma), Earth Planet. Sci. Lett., 317-318, 8-19, https://doi.org/10.1016/j.epsl.2011.11.026, 2012.

Naafs, B. D. A., Hefter, J., and Stein, R.: Millennial-scale ice rafting events and Hudson Strait Heinrich(-like) Events during the late Pliocene and Pleistocene: a review, Quaternary Sci. Rev., 80, 1-28, https://doi.org/10.1016/j.quascirev.2013.08.014, 2013.

Niu, L., Lohmann, G., Hinck, S., Gowan, E., and Krebs-Kanzow, U.: The sensitivity of Northern Hemisphere ice sheets to atmospheric forcing during the last glacial cycle using PMIP3 models, J. Glaciol., 65, 645-661, doi:10.1017/jog.2019.42, 2019.

https://doi.org/10.5194/cp-2024-10
Preprint. Discussion started: 12 February 2024

Obrochta, S. P., Crowley, T. J., Channell, J. E. T., Hodell, D. A., Baker, P. A., Seki, A., and Yokoyama, Y.: Climate variability and ice-sheet dynamics during the last three glaciations, Earth Planet. Sci. Lett., 406, 198–212, https://doi.org/10.1016/J.EPSL.2014.09.004, 2014.

Otto-Bliesner, B. L., Rosenbloom, N., Stone, E. J., Mckay, N. P., Lunt, D. J., Brady, E. C., and Overpeck, J. T.: How warm was the last interglacial? New model-data comparisons, Philos. Trans. Royal Soc. A, 371, 20130097, https://doi.org/10.1098/RSTA.2013.0097, 2013.

Parker, R. L., Foster, G. L., Gutjahr, M., Wilson, P. A., Littler, K. L., Cooper, M. J., Michalik, A., Milton, J. A., Crocket, K. C., and Bailey, I.: Laurentide Ice Sheet extent over the last 130 thousand years traced by the Pb isotope signature of weathering inputs to the Labrador Sea, Quaternary Sci. Rev., 287, 107564, https://doi.org/10.1016/j.quascirev.2022.107564, 2022.

Pattyn, F., Schoof, C., Perichon, L., Hindmarsh, R. C. A., Bueler, E., de Fleurian, B., Durand, G., Gagliardini, O., Gladstone, R., Goldberg, D., Gudmundsson, G. H., Huybrechts, P., Lee, V., Nick, F. M., Payne, A. J., Pollard, D., Rybak, O., Saito, F., and Vieli, A.: Results of the Marine Ice Sheet Model Intercomparison Project, MISMIP, Cryosphere, 6, 573–588, https://doi.org/10.5194/tc-6-573-2012, 2012.

Peltier, W. R., Argus, D. F., and Drummond, R.: Space geodesy constrains ice age terminal deglaciation: The global ICE-6G_C (VM5a) model, J. Geophys. Res. Solid Earth, 120, 450– 487, doi:10.1002/2014JB011176, 2015.

Pollard, O. G., Barlow, N. L. M., Gregoire, L. J., Gomez, N., Cartelle, V., Ely, J. C., and Astfalck, L. C.: Quantifying the uncertainty in the Eurasian ice-sheet geometry at the Penultimate Glacial Maximum (Marine Isotope Stage 6), Cryosphere, 17, 4751-4777, https://doi.org/10.5194/tc-17-4751-2023, 2023.

Pukelsheim, F.: The Three Sigma Rule, Am. Stat., 48, 88-91, https://doi.org/10.2307/2684253, 1994.

Rabineau, M., Berné, S., Olivet, J.-L., Aslanian, D., Guillocheau, F., and Joseph, P.: Paleo sea levels reconsidered from direct observation of paleoshoreline position during Glacial Maxima (for the last 500,000 yr), Earth Planet. Sci. Lett., 252, 119–137, https://doi.org/10.1016/j.epsl.2006.09.033, 2006.

Roberts, W. H. G., Valdes, P. J., and Payne, A. J.: Topography's crucial role in Heinrich Events, Proc. Natl. Acad. Sci. U.S.A, 111, 16688-16693, https://doi.org/10.1073/pnas.1414882111, 2014.

Rohling, E. J., Hibbert, F. D., Williams, F. H., Grant, K. M., Marino, G., Foster, G. L., Hennekam, R., de Lange, G. J., Roberts, A. P., Yu, J., Webster, J. M., and Yokoyama, Y.: Differences between the last two glacial maxima and implications for ice-sheet, δ18O, and sea-level reconstructions, Quaternary Sci. Rev., 176, 1–28, https://doi.org/10.1016/j.quascirev.2017.09.009, 2017.

Rutt, I. C., Hagdorn, M., Hulton, N. R. J., and Payne, A. J.: The Glimmer community ice sheet model, J. Geophys. Res. Earth Surf., 114, 2004, https://doi.org/10.1029/2008JF001015, 2009.

Sellevold, R., van Kampenhout, L., Lenaerts, J. T. M., Noël, B., Lipscomb, W. H., and Vizcaino, M.: Surface mass balance downscaling through elevation classes in an Earth system model: application to the Greenland ice sheet, Cryosphere, 13, 3193–3208, https://doi.org/10.5194/tc-13-3193-2019, 2019.

Sherriff-Tadano, S., Abe-Ouchi, A., Yoshimori, M., Oka, A., and Chan W-L.: Influence of glacial ice sheets on the Atlantic meridional overturning circulation through surface wind change, Clim. Dyn., 50, 2881–2903, https://doi.org/10.1007/s00382-017-3780-0, 2018.

Sherriff-Tadano, S., Abe-Ouchi, A., and Oka, A.: Impact of mid-glacial ice sheets on deep ocean circulation and global climate, Clim. Past, 17, 95–110, https://doi.org/10.5194/cp-17-95-2021, 2021.

Sherriff-Tadano, S., Ivanovic, R., Gregoire, L., Lang, C., Gandy, N., Gregory, J., Edwards, T. L., Pollard, O., and Smith, R. S.: Large ensemble simulations of the North American and Greenland ice sheets at the Last Glacial Maximum with a coupled atmospheric general circulation-ice sheet model, EGUsphere [preprint], https://doi.org/10.5194/egusphere-2023-2082, 2023.

Smith, R. N. B.,: A scheme for predicting layer clouds and their water content in a general circulation model, Q. J, R. Meteorol. Soc., 116, 435-460, https://doi.org/10.1002/qj.49711649210, 1990.

Smith, R.S., and Gregory, J.: The last glacial cycle: transient simulations with an AOGCM, Clim. Dyn., 38, 1545–1559, https://doi.org/10.1007/s00382-011-1283-y, 2012.

Smith, R. S., George, S., and Gregory, J. M.: FAMOUS version xotzt (FAMOUS-ice): A general circulation model (GCM) capable of energy- And water-conserving coupling to an ice sheet model, Geosci. Model Dev., 14, 5769–5787, https://doi.org/10.5194/GMD-14-5769-2021, 2021.

Snoll, B., Ivanovic, R. F., Valdes, P. J., Maycock, A. C., and Gregoire, L., J.: Effect of orographic gravity wave drag on Northern Hemisphere climate in transient simulations of the last deglaciation, Clim. Dyn., 59, 2067-2079, https://doi.org/10.1007/s00382-022-06196-2, 2022.

Stokes, C. R., Tarasov, L., and Dyke, A. S.: Dynamics of the North American Ice Sheet Complex during its inception and build-up to the Last Glacial Maximum, Quaternary Sci. Rev., 50, 86-104, https://doi.org/10.1016/j.quascirev.2012.07.009, 2012.

Stone, E.J., and Lunt, D.J.: The role of vegetation feedbacks on Greenland glaciation, Clim. Dyn., 40, 2671–2686, https://doi.org/10.1007/s00382-012-1390-4, 2013.

Svendsen, J. I., Alexanderson, H., Astakhov, V. I., Demidov, I., Dowdeswell, J. A., Funder, S., Gataullin, V., Henriksen, M., Hjort, C., Houmark-Nielsen, M., Hubberten, H. W., Ingólfsson, Ó., Jakobsson, M., Kjær, K. H., Larsen, E., Lokrantz, H., Lunkka, J. P., Lyså, A., Mangerud, J., … Stein, R.: Late Quaternary ice sheet history of northern Eurasia, Quaternary Sci. Rev., 23, 1229–1271, https://doi.org/https://doi.org/10.1016/j.quascirev.2003.12.008, 2004.

Tarasov, L., and Peltier, W. R.: Greenland glacial history and local geodynamic consequences, Geophys. J. Int., 150, 198-229, https://doi.org/10.1046/j.1365-246X.2002.01702.x, 2002.

Tarasov, L., and Peltier, W. R.: A geophysically constrained large ensemble analysis of the deglacial history of the North American ice-sheet complex, Quaternary Sci. Rev., 23, 359-388, https://doi.org/10.1016/j.quascirev.2003.08.004, 2004.

Tarasov, L., Dyke, A. S., Neal, R. M., and Peltier, W. R.: A data-calibrated distribution of deglacial chronologies for the North American ice complex from glaciological modelling, Earth Planet. Sci. Lett., 315–316, 30–40, https://doi.org/10.1016/j.epsl.2011.09.010, 2012.

Timmermann, A., Knies, J., Timm, O. E., Abe-Ouchi, A., and Friedrich, T.: Promotion of glacial ice sheet buildup 60–115 kyr B.P. by precessionally paced Northern Hemispheric meltwater pulses, Paleoceanography, 25, PA4208, doi:10.1029/2010PA001933, 2010.

Turney, C. S. M., and Jones, R. T.: Does the Agulhas Current amplify global temperatures during super-interglacials?, J. Quat. Sci., 25, 839–843, https://doi.org/10.1002/JQS.1423, 2010.

Ullman, D. J., Legrande, A. N., Carlson, A. E., Anslow, F. S., and Licciardi, J. M.: Assessing the impact of Laurentide ice sheet topography on glacial climate, Clim. Past, 10, 487–507, https://doi.org/10.5194/CP-10-487-2014, 2014

Vizcaíno, M., Lipscomb, W. H., Sacks, W. J., van Angelen, J. H., Wouters, B., and van den Broeke, M. R.: Greenland Surface Mass Balance as Simulated by the Community Earth System Model. Part I: Model Evaluation and 1850–2005 Results, J. Clim., 26, 7793–7812, https://doi.org/10.1175/JCLI-D-12-00615.1, 2013.

Waelbroeck, C., Labeyrie, L., Michel, E., Duplessy, J. C., McManus, J. F., Lambeck, K., Balbon, E., and Labracherie, M.: Sea-level and deep water temperature changes derived from benthic foraminifera isotopic records, Quaternary Sci. Rev., 21, 295–305, https://doi.org/10.1016/S0277-3791(01)00101-9, 2002.

Williams, J. H. T., Smith, R. S., Valdes, P. J., Booth, B. B. B., and Osprey, A.: Optimising the FAMOUS climate model: inclusion of global carbon cycling, Geosci. Model Dev., 6, 141–160, https://doi.org/10.5194/gmd-6-141-2013, 2013.

Williamson, D.: Exploratory ensemble designs for environmental models using k-extended Latin Hypercubes, Environmetrics, 26, 268-283, https://doi.org/10.1002/env.2335, 2015.

Ziemen, F. A., Rodehacke, C. B., and Mikolajewicz, U.: Coupled ice sheet–climate modeling under glacial and pre-industrial boundary conditions, Clim. Past, 10, 1817–1836, https://doi.org/10.5194/cp-10-1817-2014, 2014.